Mining Machines

(2023) VOLUME 41

ISSUE 4

QUARTERLY OF SCIENCE AND TECHNOLOGY

e-ISSN 2719-3306

Mining Machines

(2023) Vol. 41 Issue 4

KOMAG Research Institute

Quarterly of Science and Technology

January 30, 2024

KOMAG Institute of Mining Technology
Pszczyńska 37, 44-101 Gliwice, POLAND

miningmachines@komag.eu

e-ISSN 2719-3306

e-ISSN 2719-3306 Mining Machines, 2023, Vol. 41 Issue 4, pp. 220-230

https://doi.org/10.32056/KOMAG2023.4.1

Modeling the corrosive destruction of underground degassing pipelines

Received: 12.12.2023

Accepted: 18.01.2024

Published online: 30.01.2024

Author's affiliations and addresses:

[1] Dnipro University of Technology, 19 Yavornytskoho Ave., 49005, Dnipro, Ukraine

*** Correspondence:**

e-mail: yehorchenko.r.r@nmu.one

tel.: +38 066 383 31 66

Rostyslav YEGORCHENKO [1*], Andrii YAVORSKYI [1], Pavel DYACHKOV [1]

Abstract:

The general frequency of development of pitting corrosion was established, taking into account the results of the analysis of mine waters and foreign materials, which are favorable conditions for the formation of corrosion of steel degassing pipelines. A base of initial data was created for modeling the corrosion process of a steel degassing gas pipeline at different points in time: the beginning of the corrosion process, its development, and the end of the process. Stress distribution, corrosion potential, as well as anodic and cathodic current densities depending on the size of the corrosion crack and the longitudinal deformation of the rocks of the sole of the production was analysed. It has been proven that the high level of corrosion processes of underground pipelines is the result of the interaction of the metal, which acts as an electrode, with groundwater, which acts as an electrolyte, while the determining factors of the corrosion process are the electrical conductivity of the rocks of the bottom of the mine and the deformation processes in the pipelines. The reason of low service life of underground degassing pipelines, which are constantly exposed to mechanical and electrochemical corrosion, have been established.

Keywords: degassing, underground vacuum gas pipeline, methane-air mixture, monitoring, corrosion, output

Publisher: **KOMAG Institute of Mining Technology, Poland**

1. Introduction

An urgent task in the field of ensuring safe operating conditions of the greenhouse degassing gas pipeline is to predict the durability of the system and the formation of corrosion [1, 2]. Under the influence of an aggressive mine environment, mine degassing pipelines come into contact with aggressive fluids on their inner surface and have a short service life. The main problem that characterizes the failure of the degassing system is the critical corrosion wear of the steel segments of the gas pipeline.

To improve the quality of protective measures, predict and prevent the development of sudden emergency destruction, it became necessary to develop a model of the process of corrosion destruction of steel gas pipelines in the conditions of an aggressive mine environment [3, 4].

However, this task is little-studied and laborious in terms of execution time, as it requires the use of special approaches based on the construction of complex mathematical models of the behavior of steel degassing gas pipelines in complex mining and geological conditions of operation.

In this regard, special software have been developed, which allow to evaluate the durability of various structures in a short time. The basis of the operation of these software complexes (ABAQUS, ANSYS, COMSOL, SolidWorks, etc.) is the finite element method [5], which allows you to study the influence of external negative factors on the degassing gas pipeline and predict the formation of corrosion [6, 7]. The use of CAE systems (Computer Aided Engineering) helps designing organizations to significantly reduce designing time thus reducing the costs.

One of the widely used software packages for engineering analysis is Solid Works and COMSOL Multiphysics. Their multi-purpose orientation allows solving multi-physical tasks, such as modelling corrosion, strength under thermal load, impact of magnetic fields on the structure strength, testing the kinetics of electrochemical and chemical reactions, etc.

The aim of the work is to model the corrosion process on the degassing pipeline using Solid Works and COMSOL Multiphysics 5.6 software products.

To achieve the goal, the following tasks were solved:

- to establish patterns of changes in the profile of the mine degassing pipeline route in potentially dangerous zones of preparatory workings;
- to develop a mathematical model to determine the probability of distribution of corrosion pitting zones of a steel degassing pipeline in the conditions of an aggressive mine environment;
- to establish the maximum anodic current density under the constant impact of mechanical and electrochemical corrosion of steel degassing pipelines.

2. Methods

According to the results of diagnostics of the technical condition of mine gas pipelines and tests of the conditions of its interaction with the rock mass, it was established that in the areas of the flange joints of its segments under the impact of rock mass deformations, pipeline deflects and, as a result, zones of water accumulation, intense corrosion of the inner walls of the pipes and mechanical deposits of coal and rock dust ocurrs [8, 9].

The research work methodology includes development of a mathematical model for establishing the corrosion zones of a steel degassing pipeline and modelling the corrosion process in the conditions of a mine environment. The degassing pipeline is under the simultaneous action of a corrosive environment and permanent or temporary stresses. This process can be imagined as follows: first, local corrosion occurs on the surface of the pipe in the form of pittings, which begin to act as stress concentrators. The maximum stress will be at the bottom of the pittings, which has a more negative potential than the pipe walls, as a result of which the destruction of the metal will go deep, and the pitting itself will turn into a crack.

An aggressive environment that causes metal corrosion under normal conditions does not lead to its destruction, however, under the action of mechanical stresses, it can lead to the formation of cracks (Fig. 1).

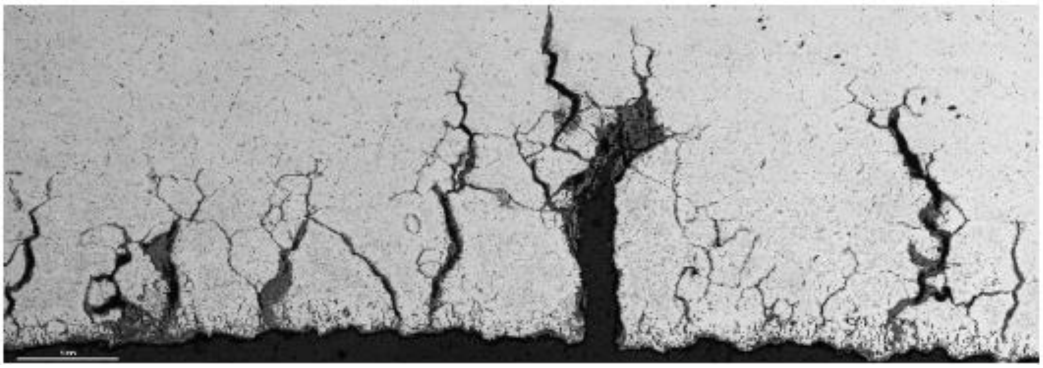

Fig. 1. Metal surface with the corrosion cracking

It should be noted that the process of corrosion fatigue of the steel links of the degassing pipeline is observed in the conditions of the mine environment. To a large extent, it is similar to how corrosion cracking occurs when static stresses are combined with corrosion. Corrosion fatigue occurs when cyclic loads are combined with corrosion. It is expressed in the destruction of metal at a significantly lower fatigue limit than in non-aggressive conditions.

Real data on the rock deformations of the bottom of the workings and modeling the technical condition of the mine degassing pipeline with the use of the SolidWorks licensed software complex, the features of the interaction of the components of the transportation and technological system of the mine gas pipeline - mine workings "ShG-GV" were established. It has been experimentally confirmed that the butt joints of the mine gas pipeline links are most susceptible to the rock mass deformations and mechanical destruction, which provokes a decrease in the output of the gas pipeline and requires development of new technical solutions for its modernization.

In accordance with the developed methodology for software modeling of mine degassing system operation modes, the elevation marks of the gas pipeline profile obtained as a result of the surveying survey became the basis for modeling the linear deformations of the pipeline under the impact of the crushed rocks of the floor.

According to the recommendations [10, 11], spatial changes of the route of the mine degassing pipeline take into account the isotropic properties and physical and mechanical characteristics of steel pipes, which are deformed in all directions equally. In this regard, deformations of the material of steel pipes in the process of spatial change of the route of the mine degassing pipeline take into account the impact of the rock mass behaviour.

3. Results

Analysis of the research work [12, 13] enabled to conclude that the operational reliability of mine degassing pipelines built in underground mine workings is influenced by the change in spatial position under the impact of deformations of the rock mass. It should be noted that underground water that enters the mine workings and the created mine space is contaminated with organic and mineral particles of varying degrees of dispersion, soluble mineral salts (including salts of heavy metals), various types of bacteria, and in some cases, they have an acidic reaction ($pH < 6$), and when in contact with moving and rotating mechanisms, they are contaminated with oil products and provoke corrosion of gas pipelines (Table 1) [14].

Table 1 shows the analysis of mine waters and their composition in various coal mining enterprises.

It should be noted that two electrochemical reactions take place on the walls of the steel gas pipeline, namely the oxidation of steel for the anodic reaction and the release of hydrogen for the cathodic reaction. This is due to aggressive mine waters, which are highly acidic.

Table 1. Composition of mine water in different mines

List of physical and chemical indicators.	Results of mine water analysis by a mine			
	"Pavlogradska"	"Im. Heroes of the Cosmos"	Western Donbas	"Blagodatna"
Suspended substances, mg/dm^3	98.80	445.00	308.20	75.1
pH	8.55	7.36	8.09	7.75
Free chlorine, mg/dm^3	-	-	-	-
General hardness, mg-eq/dm^3	36.40	161.79	116.28	45
General alkalinity, mg-eq/dm^3	4.8	1.8	2.5	-
Permanganate oxidizability, mg/dm	-	-	-	-
Dry residue, mg/dm^3	6703.50	43807.00	28497.00	14136.5
Calcium, mg/dm^3	368.81	1621.15	1175.33	430.62
Magnesium, mg/dm^3	218.87	2983.69	700.88	285.89
Total iron, mg/dm^3	1.2	0.97	0.4	0.89
Chlorides, mg/dm^3	2642.97	22314.94	15351.41	8022.7
Sulfates, mg/dm^3	576.36	441.88	365.03	577.17
Petroleum products, mg/dm^3	0.75	0.65	0.63	0.8

It is known that the high level of corrosion processes of steel pipelines is the result of the interaction of the metal, which acts as an electrode, with groundwater as an electrolyte, and the determining factor of the corrosion process is the soil electrical conductivity. Electrochemical corrosion often has a local character, that is, it causes areas of corrosion and caverns of great depth on the pipeline, which can turn into fistulas in the pipe wall. Such corrosion is much more dangerous than continuous corrosion [15, 16].

The initial parameters (Table 1) were included in the mathematical model to determine the probability of the distribution of corrosion pitting zones for the first model and modeling the electrical conductivity of the soil under the influence of deformation, which lead to stresses in the pipelines for the second model.

The first model showed the frequency of development of pitting corrosion, taking into account the results of the analysis of mine water and foreign materials, which create favourable conditions for the corrosion process.

The degassing pipeline, which is curved in the profile and consists of 6 sections of pipes with a length of 4.0 m, diameter of 300 mm and a wall thickness of 4.0 mm, was selected as the tested object. Degassing pipes supplied to mines are made of typical carbon steel without a special coating.

Let's consider the first model of the formation process of pitting corrosion.

Papers [17-19] proposed the dependence of the formation of pitting corrosion on the content of chlorine ions in the mine water, which contribute to destruction corrosion of steel. The pitting potential is calculated using the following expression:

$$E_{po} = \Delta E_{po} + E_{cor}, \tag{1}$$

where:

E_{po} – pitting potential, V,

E_{cor} – corrosion potential, V,

ΔE_{po} – basis of pitting resistance.

$$E_{po} = b + a \cdot \log|Cl^-|, \quad (2)$$

where:

a, b – constants,

$|Cl^-|$ – concentration of chlorine ions.

It should be noted that the coefficients a, b are unknown to us, and their determination required a linear approximation based on known chloride ion concentrations from the work [20]. As a result, the following value was set for our initial concentration of Cl^- (table 1).

E_{cor} = -1.303 V.

The probability of pitting formation from the moment of starting the model Po(t) is calculated by the following expression:

$$P_0(t) = P_0(\tau \geq t), \quad (3)$$

$$P_0(t + dt) = P_0(t)P_0(dt) = P_0(t)(1 - \lambda dt)\,, \quad (4)$$

According to expressions (3, 4), we get that the change in Po(t) depends on the probability of formation of single pitting λ, according to the following recommendations

$$\frac{dP_0}{dt} = -\lambda P_0(t) \quad (5)$$

By solving equation (5), we get:

$$P_0(t) = \exp(-\lambda t), \quad (6)$$

where:

$P_o(t)$ – dependence of the probability of pitting formation on time,

t – time since model initialization,

λ – probability of formation of single pitting.

The average time of the moment of the beginning of pitting formation τ is defined as:

$$\tau = \frac{\int_0^\infty texp(-\lambda t)dt}{\int_0^\infty exp(-\lambda t)dt} = \frac{1}{\lambda}, \quad (7)$$

The obtained values were used as a base of initial data with introduction of relevant equations into the model, on the basis of which models of the profile of the degassing pipeline were built at different points in time (Fig. 2): the beginning of the corrosion process, its development and the end of the process. The period of observation of the sample was 3 months, the length of the cut was 1000 mm.

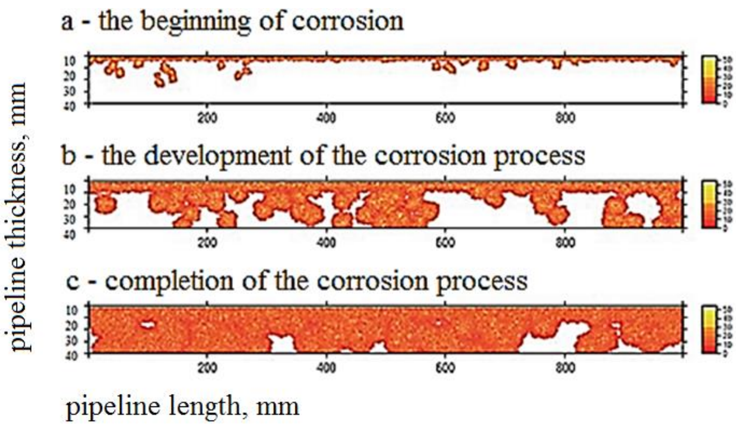

Fig. 2. Change in the dynamics of pitting corrosion depending on the time interval of contact with an aggressive environment

Modeling the electrical conductivity of the soil under the impact of deformation, which leads to stresses in pipelines, was considered in the second model. The physical and mechanical properties of the material of the degassing pipes considered in the generated CAD models are presented in Table 2.

Table 2. Basic properties of carbon steel

Properties	Value	Unit
Modulus of elasticity	$2{,}1 \cdot 10^{11}$	N/m^2
Shear modulus	$7{,}9 \cdot 10^{10}$	N/m^2
Mass density	7800	kg/m^3
Tensile strength limit	399826000	N/m^2
Poisson's ratio	0,28	
Liquidity limit	220594000	N/m^2
Coefficient of thermal expansion	$1{,}3 \cdot 10^{-5}$	
Thermal conductivity	43	W/(m·K)
Specific heat capacity	440	J/kg·K

The simulation was carried out using the Solid Works licensed software complex and the COMSOL Multiphysics 5.6 product, which made it possible to test distribution of stresses, the corrosion potential, as well as the anodic and cathodic current densities depending on the size of the corrosion crack and the longitudinal deformation of the floor rocks (Fig. 3)

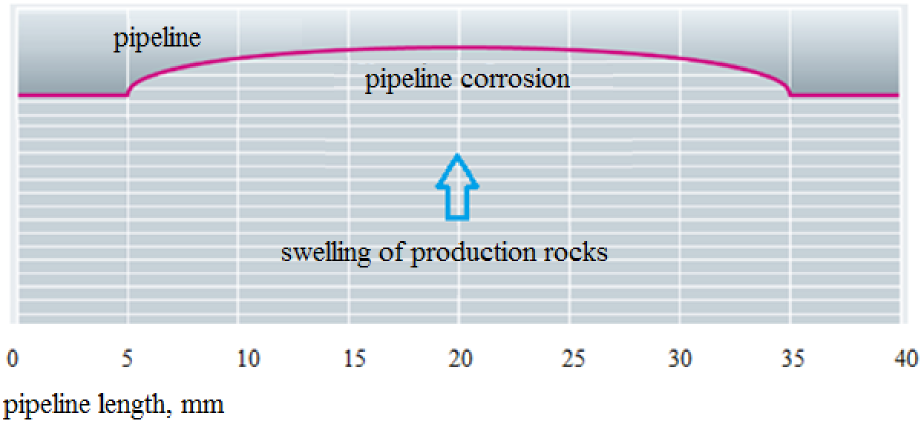

Fig. 3. Geometric model of a pipeline with a corrosion defect

Elastic-plastic stresses in a gas pipeline steel was modelled using the model of plasticity at small deformations and the von Mises flow criterion [21, 22].

The SolidWorks interface and a user-defined isotropic hardening model were used for modelling. The function σ_{yhard} was defined as:

$$\sigma_{yhard} = \sigma_{exp}\left(\varepsilon_{eff}\right) - \sigma_{ys} = \sigma_{exp}\left(\varepsilon_p + \frac{\sigma_e}{E}\right) - \sigma_{ys}, \tag{8}$$

where:

σ_{exp} – the experimental stress function obtained from the measured stress-strain curve of steel,
ε_{eff} – total effective strain,
σ_{ys} – the yield strength of steel is $803 \cdot 10^6$ Pa,
ε_p – plastic deformation,
σ_e – von Mises stress,
E – Young's modulus of elasticity equal to $207 \cdot 10^9$ Pa,
$\frac{\sigma e}{E}$ – elastic deformation.

Publisher: **KOMAG Institute of Mining Technology, Poland**

In the process of corrosion cracking, two electrochemical reactions take place [23] (and it is assumed that only the surface of the corrosion crack is electrochemically active):

1. anodic - dissolution of iron ($Fe \rightarrow Fe^{+2}+ 2e$);
2. cathodic – release of hydrogen ($2H_2O+ 2e \rightarrow H_2 +2OH^-$).

The anodic Tafel expression of the following form was used to model the iron dissolution reaction:

$$i_a = i_{0,a} 10^{\frac{\eta_a}{A_a}} \tag{9}$$

where:

$i_{0,a}$ – exchange current density ($2.353 \cdot 10^{-3}$ A/m^2),

A_a – the slope of the Tafel curve (0.118 V), and the overvoltage η_0 for the anodic reaction is calculated by the following formula:

$$\eta_a = \phi_s - \phi_l - E_{cq,a}, \tag{10}$$

where:

ϕ_s, ϕ_l – electrostatic potential.

and the equilibrium potential of the anodic reaction $E_{cq,a}$ is calculated from the following formula:

$$E_{cq} = E_{cq0} - \frac{\Delta P_m V_m}{zF} - \frac{TR}{zF} \ln\left(\frac{\upsilon\alpha}{N_0}\varepsilon_p + 1\right), \tag{11}$$

where:

E_{cq0} – standard equilibrium potential of the anodic reaction (−0.859 V),

ΔP_m – excess pressure to elastic deformation ($2.687 \cdot 10^8$ Pa),

V_m – molar volume of steel ($7.13 \cdot 10^{-6}$ m^3/mol),

z – charge number for steel (2),

F – Faraday constant,

T – absolute temperature (298.15 K),

R – ideal gas constant,

ν – coefficient depending on the orientation (0.45),

α – coefficient ($1.67 \cdot 10^{15}$ m^{-2}),

N_0 – initial density of dislocations ($1 \cdot 10^{12}$ m^{-2}).

Tafel's cathodic expression was used to model the iron dissolution reaction, it establishes the local cathodic current density.

$$i_c = i_{0,c} 10^{\frac{\eta_c}{A_c}} \tag{12}$$

where:

$i_{0,c}$ – exchange current density,

A_c – the Tafel slope (−0.207 V), and the overvoltage ηc (V) for the cathodic reaction is calculated by the formula

$$\eta_a = \phi_s - \phi_l - E_{cq,c} \tag{13}$$

where:

$E_{cq,c}$ – standard equilibrium potential of the cathodic reaction (-0.644 V).

The exchange current density for the cathodic reaction was determined by the following formula:

$$i_{o,c} = i_{0,c,ref} 10^{\frac{\sigma_e V_m}{6(-A_c)}} \tag{14}$$

where:

$i_{0,c,ref}$ – eference exchange current density for the cathodic reaction without external stress ($1.457 \cdot 10^{-2}$ A/m^2)

The simulation was carried out in several stages: at the first stage, the types of physical solvers (solid mechanics and secondary current distribution) and the type of calculation (stationary) were selected. At the second stage, the geometric model of the underground pipeline with an elliptical crack (Fig. 3) was constructed, the model of isotropic hardening, the parameters of the electrochemical corrosion process, the mechanical properties of the pipeline material, the amount of longitudinal deformation of the pipeline, etc. were specified. At the third stage, a grid of finite elements was constructed and the von Mises stress distribution was calculated, as well as the distribution of corrosion potential, anodic and cathodic current densities along the length of the corrosion crack, depending on the degree of longitudinal deformation

Impact of longitudinal movements of the soil on the corrosion process of underground degassing pipelines has been demonstrated using various possible deformations of the pipeline [24, 25]. The Mises background voltage in the steel pipe, the electrolyte potential distribution, and the direction of the current in the surrounding soil are shown in Fig. 4.

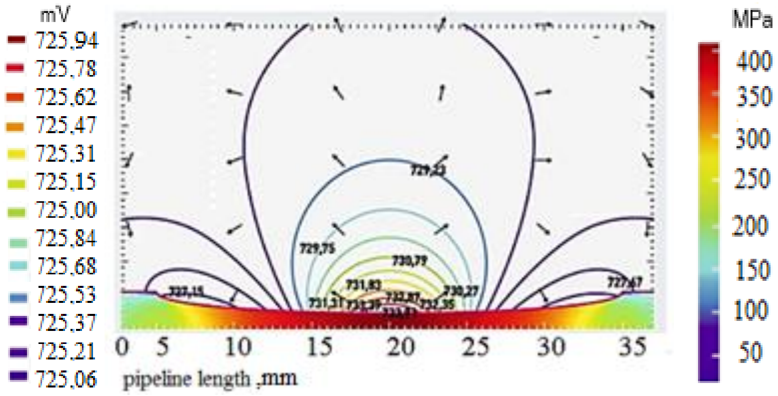

Fig. 4. Distribution of stress in the pipeline according to von Mises (MPa), electrolyte potential (mV) and current line in the soil

Fig. 4 presents the Mises background stresses, which increase with the increase of possible deformations of the pipeline and are maximal in the center of the corrosion defect and reach 300 and 350 MPa.

It should be noted that the electrolyte potential distribution is uneven near the corrosion defect. Arrows along the lines of current indicate the direction and distribution of current density in the soil.

A comparative analysis of the von Mises stress distribution results by the length of the corrosion defect for each strain value is shown in Fig. 5 a. It can be seen that the stresses increase with increasing tensile strain and are maximal in the center of the corrosion defect. For deformations of 2.0 and 2.25 mm, the local stress in the center of the corrosion defect exceeds the yield strength of high-strength alloy steel (403 MPa). This leads to plastic deformation in the center of the corrosion defect, while in the other area the corrosion defect remains in the elastic range.

Fig. 5 b shows the distribution of the electrode corrosion potential and the anodic and cathodic current densities along the length of the corrosion defect.

The graph of the local potential of the electrode along the length of the corrosion defect confirms that the even distribution changes to an uneven distribution with increasing the tensile strain, and a greater negative corrosion potential, in absolute value. is achieved in the center of the corrosion defect unlike at both edges. This effect is explained by the large absolute value of the negative potential of the equilibrium anodic reaction in the area of plasticity of the defect at the highest possible longitudinal deformations.

Increase in anodic current density for tensile strains of 2.0 and 2.25 mm is explained by the plastic deformation observed in the center of the corrosion defect (Fig. 5 c). The strongest negative current is found in the center of the corrosion defect, where the distribution of the cathodic current density is the most uneven for a tensile strain of 2.25 mm (Fig. 5 d).

Total current density is a sum of the anodic and cathodic current densities, and for deformations of 2.0 and 2.25 mm, the total current density in the center of the corrosion defect is determined mainly by the anodic current density, and on both sides of the defect by the cathodic current density. Therefore, the distribution of the total current density is uneven for large tensile strains, and the direction of the current near the corrosion defect changes to the opposite.

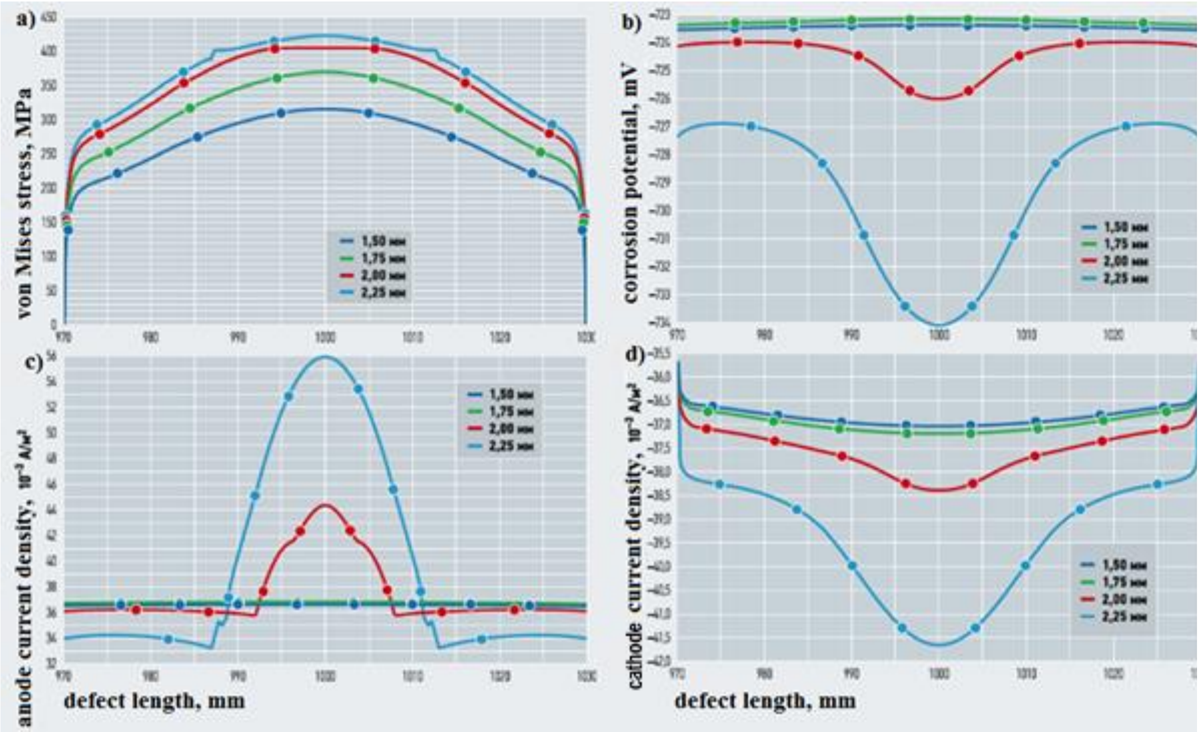

Fig. 5. Distribution of electrode's corrosion potential and anodic and cathodic current densities along the length of the corrosion defect

The results show that the higher deformations of the pipeline, caused by the deformation of the floor rocks, which lead to plastic deformation in the zone of the corrosion defect of the steel pipe and thereby to a greater absolute value of the negative potential of the local electrode and a higher density of the anodic current increase corrosion of the pipeline. This is one of the reasons for the short service life of underground degassing pipelines, which are under the constant impact of mechanical and electrochemical corrosion.

4. Conclusions

The modeling of corrosion failure showed that starting from a crack depth of 2 mm, the process of plastic deformation of the gas pipeline material at the crack tip starts. As the stress intensity factor increases, the crack growth rate increases. Starting from a crack depth of 3 mm, the probability of failure in the form of a mechanical break at an angle of 45º towards the hoop tensile stresses increases. When a depth of 4 mm is reached, the stress from the inner wall of the gas pipeline will exceed the yield strength of the material, which can lead to unstable operation with a subsequent accident. Consequently, safe operation of this gas pipeline is possible when the defect depth is less than 50% of the wall thickness, depending on the length. Defects with a depth of 50% or more are unacceptable, regardless of length.

The results of modeling and testing the underground pipelines corrosion process using the software products such as SolidWorks and COMSOL Multiphysics established that the degassing network of mines is constantly under the impact of mechanical-electrochemical interaction, which manifests itself in the longitudinal deformations of the mine floor rocks.

High intensity of corrosion in underground pipelines is the result of the interaction of the metal, which acts as an electrode, with groundwater, which acts as an electrolyte, while the electrical conductivity of the soil and the deformation processes in the pipelines are the determining factors of the corrosion process.

The primary corrosion protection of pipelines of underground degassing pipelines can be the improvement of the methods for control and the technical maintenance of mine degassing pipelines to eliminate mechanical deformations and impact of aggressive groundwater.

References

[1] Kononenko M., Khomenko O., Myronova I. & Kovalenko I. (2022). Economic and environmental aspects of using mining equipment and emulsion explosives for ore mining. Mining Machines, 40(2), 88-97. https://doi.org/10.32056/KOMAG2022.2.4

[2] Khomenko O., Kononenko M., Myronova I., Kovalenko I., Cabana Edgar Cáceres & Dychkovskyi R. (2023). Technology for increasing the level of environmental safety of iron ore mines with use of emulsion explosives. Mining Machines, 41(1), 48-57. https://doi.org/10.32056/KOMAG2023.1.5

[3] Shirin, L., Bartashevsky, S., Denyshchenko, O. & Yegorchenko, R. (2021). Improving the capacity of mine degassing pipelines. Naukovyi visnyk natsionalnoho hirnychoho universytetu, 6, 72 – 77. https://doi.org/10.33271/nvngu/2021-6/072

[4] Yegorchenko, R., Mukha, O. & Shirin., L. (2022). The methods to calculate expediency of composite degassing pipelines. Naukovyi visnyk natsionalnoho hirnychoho universytetu, №4. 23-27. https://doi.org/10.33271/nvngu/2022-4/023

[5] Shirin, L. N., & Yegorchenko, R. R. (2022). Modeling the minds of the interaction of elements of the transport-technological system “mine gas pipeline – mining plant”. Oil and Gas Power Engineering, 1(37), 88–96. https://doi.org/10.31471/1993-9868-2022-1(37)-88-96

[6] Mensah, A., & Sriramula, S. (2024). Probabilistic finite element-based reliability of corroded pipelines with interacting corrosion cluster defects. International Journal of Pressure Vessels and Piping, 207, 105086. https://doi.org/10.1016/j.ijpvp.2023.105086

[7] Jiang, F., & Dong, S. (2024). Probabilistic-based burst failure mechanism analysis and risk assessment of pipelines with random non-uniform corrosion defects, considering the interacting effects. Reliability Engineering & System Safety, 242, 109783. https://doi.org/10.1016/j.ress.2023.109783

[8] Mineev, S.P., Pymonenko, D.M., Novikov, L.A. & Slashchev, A.I.(2019). Some features of transportation and processing of methane-air mixture in coal mines. Collection of scientific works of the National Mining University. Dnipro Vol. 59. P. 98-107. https://doi.org/10.33271/crpnmu/59.098

[9] Yegorchenko, R. R., Oksen, Yu. I., & Shirin, L. N. (2022). Modeling the flow of a methane-burning mixture with degassing gas pipelines of a folding configuration. Prospecting and Development of Oil and Gas Fields, 2(83), 54–62. https://doi.org/10.31471/1993-9973-2022-2(83)-54-62

[10] Milenin, A., Velikoivanenko, E., Rozynka, G., & Pivtorak, N. (2023). Numerical analysis of brittle strength of welded pipelines with corrosion metal loss in transportation of blends of natural gas with hydrogen. https://doi.org/10.21203/rs.3.rs-3303744/v1

[11] Dong, L., ZHANG, S., Gan, T., Qiu, Y., Song, Q., & Zhao, Y. (2023). Frequency Characteristics Analysis of Pipe-to-Soil Potential Under Metro Stray Current Interference Using Continuous Wavelet Transform Method. https://doi.org/10.2139/ssrn.4487556

[12] Sofiyskiy, K.K., Stasevich, R.K., Pritula, D.A. & E.E. Dudlya. (2016). Improving safety of transportation, extraction and utilization of methane of surface decontaminating wells. Geotechnical Mechanics. Dnipropetrovsk. VIP. 128p. 216

[13] Maznytskyi, A. S., Starovyerov, V. S. &Nikitenko K. O. (2019). An integral assessment of the impact of geological factors on the reliability of the operation of the main gas pipeline "Urengoi-PomariUzhhorod". Urban planning and territorial planning: Nac.-techn. zb. Answer ed. M. M. Ossetrin. K.: KNUBA. Vol. 70. P. 516-527

[14] Trus. I. M., Grabitchenko, V. M. & Petrychenko A. I. (2012). Purification of highly mineralized mine waters from sulfates using lime and metallic aluminum. Bulletin of KrNU. Kremenchuk: KDPU. Vol. 2 (14). C. 77–79

[15] Wang, M., Tan, M. Y., Zhu, Y., Huang, Y., & Xu, Y. (2023). Probing top-of-the-line corrosion using coupled multi-electrode array in conjunction with local electrochemical measurement. Npj Materials Degradation, 7(1). https://doi.org/10.1038/s41529-023-00332-x

[16] Zhang, C., Wang, H., He, Y., Zheng, W., & Wang, Y. (2023). Electrochemical potential dependence of SCC initiation in X60 pipeline steel in near-neutral pH environment. Journal of Materials Research and Technology, 27, 4950–4961. https://doi.org/10.1016/j.jmrt.2023.10.213

[17] N. N. Sergeev, S. N. Kutepov, A. N. Sergeev, A. G. Kolmakov, V. V. Izvol'skii, A. E. Gvozdev. (2020). Long-Term Strength of 22Kh2G2AYu Reinforcing-Bar Steel during Corrosion Cracking Tests in a Boiling Nitrate Solution // Russian Metallurgy (Metally).. № 4. P.434-440

[18] Gvozdev, A. E. (2019). Extreme effects of strength and plasticity in metal highly alloyed ingot and powder systems: monograph. 2nd ed., correct. and additional Tula: TulSU Publishing House. p. 477

[19] Moran, A. J., & Lillard, R. S. (2023). A Modeling Approach to Understanding the Interrelated Nature of Cathodic Protection Current and AC Stray Current on Pipelines. Corrosion, 79(5), 526–538. https://doi.org/10.5006/4272

[20] Kuzmenko, O., Dychkovskyi, R., Petlovanyi, M., Buketov, V., Howaniec, N., & Smolinski, A. (2023). Mechanism of Interaction of Backfill Mixtures with Natural Rock Fractures within the Zone of Their Intense Manifestation while Developing Steep Ore Deposits. Sustainability, 15(6), 4889. https://doi.org/10.3390/su15064889

[21] COMSOL Multiphysics: Corrosion Module. User's Guide. 2019. p. 428

[22] COMSOL Multiphysics: Structural mechanics module. User's Guide. 2019. p. 1406

[23] Pradhan, S. K., Bhuyan, P., & Mandal, S. (2018). Individual and synergistic influences of microstructural features on intergranular corrosion behavior in extra-low carbon type 304L austenitic stainless steel. Corrosion Science, 139, 319–332. https://doi.org/10.1016/j.corsci.2018.05.014

[24] Kononenko, M., Khomenko, O., Kovalenko, I., Kosenko, A., Zahorodnii, R., & Dychkovskyi, R. (2023). Determing the performance of explosives for blasting management. Rudarsko-Geološko-Naftni Zbornik, 38(3), 19–28. https://doi.org/10.17794/rgn.2023.3.2

[25] Shirin, L.N., Yegorchenko, R.R., & Taran, V.O. (2022). Monitoring and operational control of the formation of gas hydrates in degassing pipelines. Collection of scientific works of NSU. – Dnipro: NTU "Dniprov Polytechnic". No. 69 - p. 243 – 253. https://doi.org/10.33271/crpnmu/69.243

Publisher: **KOMAG Institute of Mining Technology, Poland**

e-ISSN 2719-3306 Mining Machines, 2023, Vol. 41 Issue 4, pp. 231-239

https://doi.org/10.32056/KOMAG2023.4.2

Legal and technical considerations for testing and certification of CHP units

Received: 15.12.2023

Accepted: 15.01.2024

Published online: 30.01.2024

Author's affiliations and addresses:

[1] KOMAG Institute of Mining Technology, Pszczyńska 37, 44-101 Gliwice, Poland

*** Correspondence:**

e-mail: afigiel@komag.eu

Andrzej FIGIEL [1*], Andrzej NIEDWOROK [1]

Abstract:

Cogeneration units, which generate heat and electricity using the same technological process, and which transmit their surplus electricity to the electricity grid, are subject to the provisions of Commission Regulation (EU) 2016/631 of April 14, 2016 establishing a network code on requirements for grid connection of generators (NC RfG). The article discusses the legal and technical conditions for cogeneration units, which were established in particular to ensure the safety of electricity supply. It also presents the procedure and rules for confirming the compliance of cogeneration units with the technical requirements of the Network Code mentioned above on the basis of tests and certification carried out at the KOMAG Institute.

Keywords: Combined Heat and Power, power generation units, network code, testing, certification

Publisher: **KOMAG Institute of Mining Technology, Poland**

1. Introduction

According to the European Climate Law, adopted by the European Parliament as part of the European Green Deal, greenhouse gas emissions should be reduced by at least 55% by 2030 and carbon neutrality, also known as climate neutrality, or net zero emissions, meaning a balance between CO_2 emissions and CO_2 uptake from the atmosphere, should be achieved in 2050 [1].

Achieving the above-mentioned goals requires taking action to develop clean energy sources, reduce emissions from the energy sector (fuel combustion is responsible for more than 3/4 of greenhouse gas emissions in the European Union) and reduce energy consumption.

Simultaneous generation of heat and electricity during the same technological process makes it possible to achieve efficiencies in excess of 90%, while the efficiency of generating only electricity does not exceed 40% [2].

Cogeneration units that generate heat and electricity during the same technological process, and that transfer their surplus electricity to the power grid, are subject to the provisions of the Commission Regulation (EU) 2016/631 of 14 April 2016 establishing a network code on requirements for grid connection of generators (NC RfG) [3].

The establishment of the NC RfG Code was aimed at ensuring fair competition conditions in the European Union's internal electricity market, maintaining security of energy supply and integration of renewable sources of electricity. Power generating units, including cogeneration units, should meet the technical requirements of connection to the transmission and distribution system, so that they are characterized by an adequate response to deviation from the reference voltage and rated frequency, are immune to disturbance conditions in the system, and enable easy restoration of operation after a breakdown.

All new generating units, including CHP units, added into operation must meet the requirements of the NC RfG Code. In order to verify that generating units meet the technical requirements of the NC RfG Code, they should be certified by accredited certification bodies. Electricity system operators allow a certified generating unit to be connected to the grid without hindrance. Anticipating the need for the implementation of the NC RfG code in Poland, the KOMAG Institute has taken measures resulting in the construction of a research infrastructure, the implementation of research methods (Applied Research Laboratory) and a certification programme (Attestation Testing Department Certification Unit), allowing comprehensive testing and certification of generating units.

The KOMAG Institute, as the first organization in Poland, was accredited by the Polish Accreditation Centre for testing and certification of manufacturing units based on the criteria of the NC RfG network code.

2. Requirements for CHP units connected to the power grid

According to the NC RfG Code, CHP units, depending on their maximum generating capacity and voltage level at the point of connection, can be classified into one of four types of power-generation modules, designated as Type A, B, C and D (Table 1). Proposals for maximum power thresholds for type B, C and D generation modules are subject to approval by the relevant regulatory authority or, if applicable, by the member state. In Poland, the values proposed by national distribution system operators were approved by the President of the Energy Regulatory Office (ERO) - Decision of the President of the Energy Regulatory Office DRE.WOSE.7128.184.3.2018.ZJ dated July 16, 2018 [4].

Publisher: **KOMAG Institute of Mining Technology, Poland**

Table 1. Voltage level limits and maximum power thresholds for power-generating modules of types A, B, C, D

Type of generation unit (power generation module)	**A**	**B**	**C**	**D**
Voltage at the connection point	< 110 kV	< 110 kV	< 110 kV	≥ 110 kV
Maximum power threshold limit in Continental Europe	0.8 kW	1 MW	50 MW	75 MW
Maximum power threshold limit in Poland	0.8 kW	0.2 MW	10 MW	75 MW

The requirements of the NC RfG code for different types of power generation modules vary. In practice, cogeneration units that generate electricity and heat from the combustion of gaseous fuel (biogas, natural gas) or liquid fuel (bioliquids, diesel) can be classified as Type A modules (voltage lower than 110 kV, power not exceeding 200 kW) or Type B (voltage lower than 110 kV, power not exceeding 10 MW).

For CHP units categorized as Type A power generation modules, the requirements apply at the basic level, the achievement of which is necessary to ensure generation capacity with limited automatic response and minimal regulation by the system operator. The requirements for Type B power generation modules apply to a broader range of automatic, dynamic response to mitigate the effects of system events and provide a higher level of regulation by the system operator.

CHP units of type A and type B shall meet the technical requirements listed in Table 2.

Table 2. Requirements for cogeneration units type A and type B

No.	**Requirement**	**NC RfG Code**	**Module type**	
			A	**B**
1	Capability of remaining connected to the network and operate within the frequency ranges and frequency ranges and time periods specified in Article 13(1)(a)(i) of the NC RfG Code for the synchronous area - Continental Europe	Article 13(1) (a)(i)	X	X
2	Capability of staying connected to the network and operate at rates of frequency change (RoCoF – ang. Rate of Change of Frequency), df/dt.	Article 13(1) (b)	X	X
3	Capability of power-generating module of activating the provision of active power frequency response at a frequency threshold and droop settings specified by the relevant TSO[1]	Article 13(2) (a)(c)(d)(e)(f) (g)	X	X
4	Admissible active power generation reduction with a decrease in frequency.	Article 13(4)	X	X
5	Cease active power output within five seconds following an instruction being received at the input port (logical interface).	Article 13(6)	X	X
6	Capability of connecting automatically to the network - frequency ranges within which an automatic connection is admissible, the corresponding delay time and maximum admissible gradient of increase in active power output.	Article 13(7)	X	X
7	Regulation of active power output by the relevant system operator using instructions via the input port (logical interface).	Article 14(2)	-	X
8	Capability to staying connected to the network and continuing to operate stably after the power system has been disturbed by secured faults on the transmission system.	Article 14(3)	-	X

[1]TSO – transmission system operator

The following part of the article discusses how testing and certification of CHP units - processes conducled by an accredited testing laboratory and accredited certification body of the KOMAG

Institute, whose purpose is to verify compliance with the above-mentioned requirements of the NC RfG Code, are carried out.

3. KOMAG Institute's activities with regard to testing and certification of CHP units

The KOMAG Institute has actively engaged in activities aimed at reducing greenhouse gas emissions, promoting "green" technologies and environmental protection. One of these activities was the establishment in 2021 of a testing infrastructure at the Applied Research Laboratory, which allows the implementation of comprehensive testing of power generating units connected to the electricity grid, resulting from the Commission Regulation (EU) 2016/631 of April 14, 2016. (NC RfG Code).

The testing infrastructure was created mainly with the aim of conducting tests on photovoltaic inverters, inverters working with hydroelectric and wind turbines. It quickly became apparent that the laboratory's testing and organizational potential could be successfully used to test CHP units.

The Applied Testing Laboratory was the first laboratory in Poland to be accredited by the Polish Centre for Accreditation (accreditation certificate AB 665) to perform tests on power generating units with a rated power of up to 250 kW, in accordance with the requirements of the Commission Regulation (EU) 2016/631 of April 14, 2016 and the conditions [5] set by the Polish Power Transmission and Distribution Association (PTPiREE) – an association of the Distribution Network Operators and the Transmission Network Operator and energy industry employees.

As a natural consequence of the laboratory's extension of the scope of accreditation, the Division of Attestation Tests, Certifying Body (accreditation certificate AC 023) - a separate certification unit within the Institute - implemented a certification programme and was accredited by the Polish Centre for Accreditation.

Certification of power generating units (power generating modules) is carried out according to the following reference documents:

- Commision Regulation (EU) 2016/631 of 14 April 2016 establishing a network code on requirements for grid connection of generators - acronym of the document NC RfG [3],
- General Application Requirements resulting from the Commission Regulation (EU) 2016/631 of April 14, 2016 establishing a network code on requirements for grid connection of generators - approved by the decision of the President of the Energy Regulatory Authority DRE.WOSE.7128.550.2.2018.ZJ dated 2 January 2019 [6],
- Standard PN-EN 50549-1:2019-02 [7].

Certificates of conformity are issued by the Division of Attestation Tests, Certifying Body primarily on the basis of current measurements of physical characteristic related to the verified property of the tested power generating unit. The test results that are the basis for the issuance of a certificate of conformity are documented in the test report, which is made available to the appropriate network operator upon request.

Certificates of compliance are the basis for including the certified device in the list [8] managed by the Polish Electricity Transmission and Distribution Association and thus obtaining a permit to connect the device to the power grid.

4. Testing of CHP units

Testing of CHP units is carried out in accordance with the programme established by the certification body. The programme refers to the technical requirements of the NC RfG Code listed in Table 2. Part of the testing can be performed by the laboratory's specialists at the manufacturer's site, using the manufacturer's infrastructure, usually due to the need to provide an adequate amount of fuel. The test object is a certified product or a sample representative of a series of products. An example of a CHP unit subjected to testing at the KOMAG Institute is shown in Fig. 1.

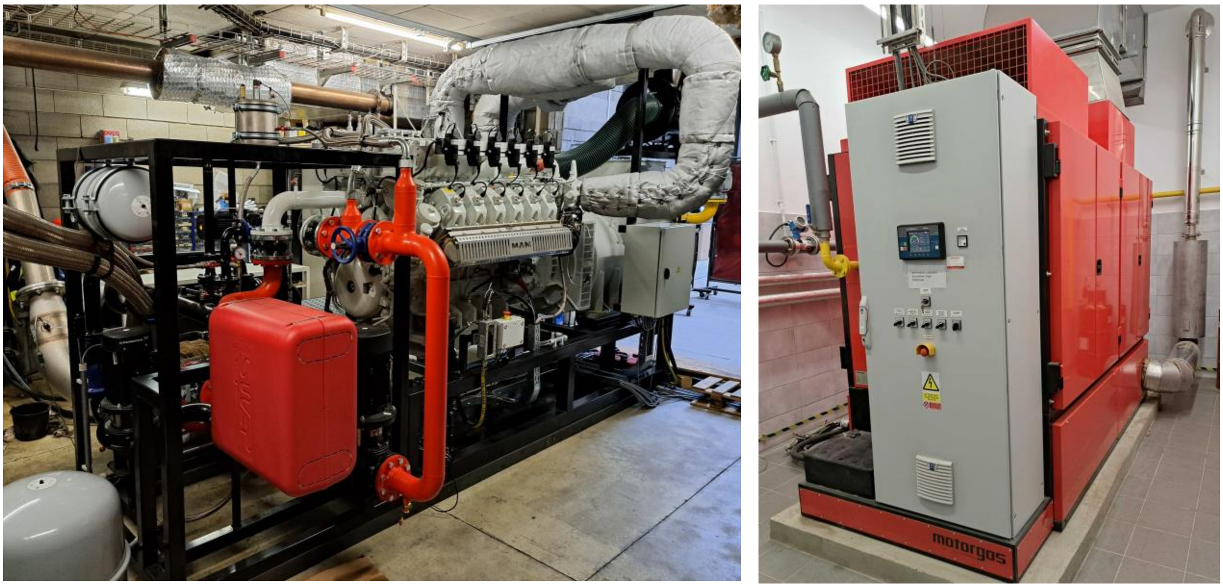

Fig. 1. CHP unit (example)

Testing of CHP units is carried out in the Applied Research Laboratory in the configuration shown in Fig. 2. Electrical parameters at the point of connection of the unit to the grid (under laboratory conditions to the grid simulator) are measured and recorded.

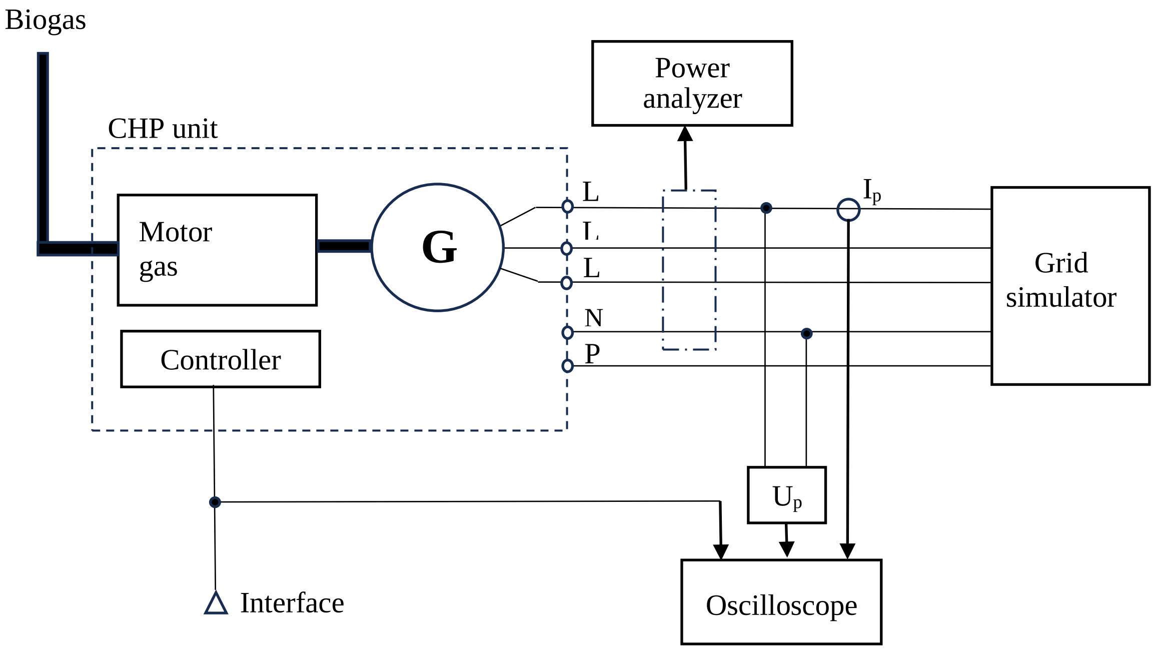

Fig. 2. Schematic of the system for testing CHP units

The values obtained during the tests are recorded and analyzed in terms of meeting the requirements of the NC RfG Code, General Application Requirements (PSE) as well as PN-EN 50549-1:2019-02.

The charts below show selected sample test results, the object of which was a CHP unit.

a) Tests of power response to increased frequency (LFSM-O).
   Requirement: Article 13, paragraph 2 - NC RfG and item 4.6.1 of EN 50549-1:2019-02.

Publisher: **KOMAG Institute of Mining Technology, Poland**

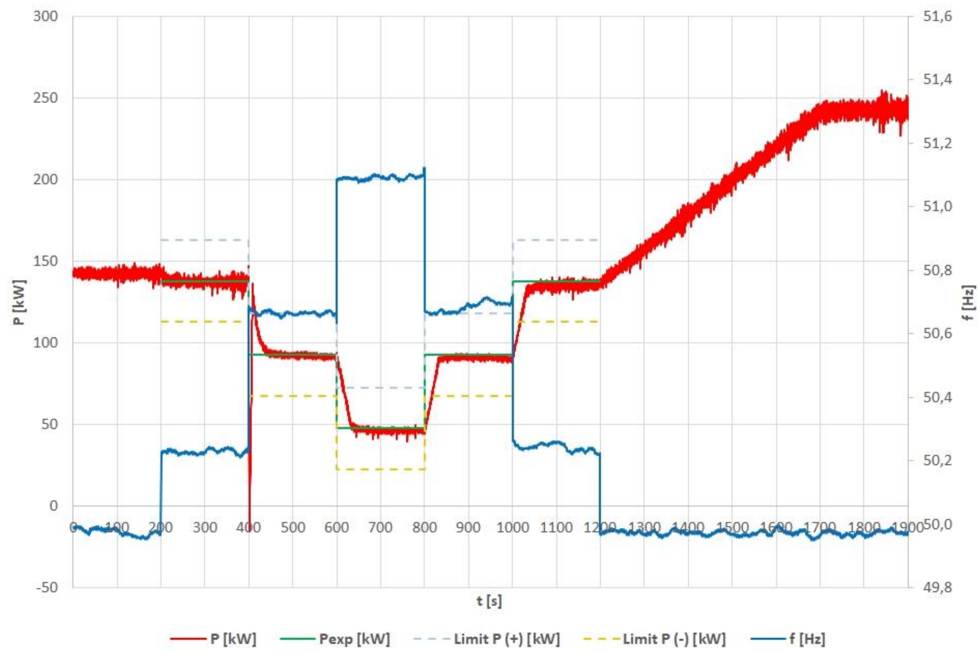

Fig. 3. Time diagram of P_{EUT}, f_{EUT} for active power response tests at increased frequency (f_1 = 50,2 Hz, f_{stop} = 50,2, s = 5%, Pset > 60% Pn)

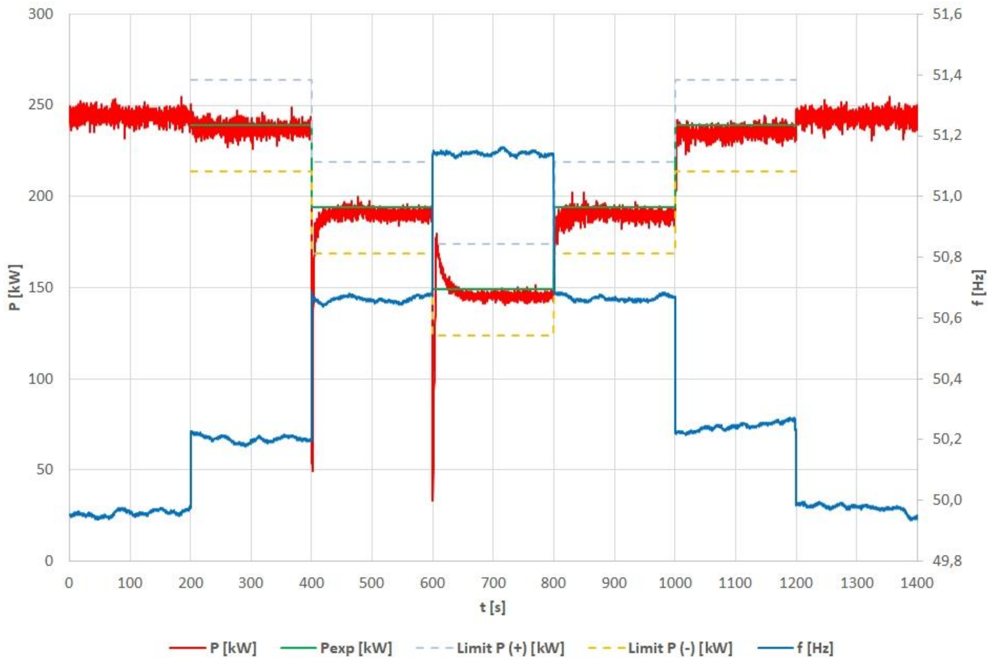

Fig. 4. Time diagram of P_{EUT}, f_{EUT} for active power response tests at increased frequency (f_1 = 50,2 Hz, f_{stop} = 50,2, s = 5%, Pset > 100% Pn)

b) Cease active power output within five seconds following an instruction being received at the input port (logical interface).

Requirement: Article 13, paragraph 2 - NC RfG and item 4.6.1 of EN 50549-1:2019-02.

The test is designed to verify the functionality of the CHP unit to stop active power generation after receiving the applied command on the available logical interface. Testing is performed for all available logical interfaces, such as binary input or MODBUS protocol, based on RS485

(MODBUS ASCII or RTU) and Ethernet (MODBUS TCP) interfaces. The condition that confirms proper operation is the cessation of active power generation (phase current decay) within five seconds of receiving a command.

Fig. 5. A diagram illustrating the time to stop active power generation after accepting a command at the input port (logical interface)

c) Regulation of active power output by the relevant system operator using instructions via the input port (logical interface).

Requirement: Article 14, paragraph 2 - NC RfG and item 4.11.2 of EN 50549-1:2019-02.

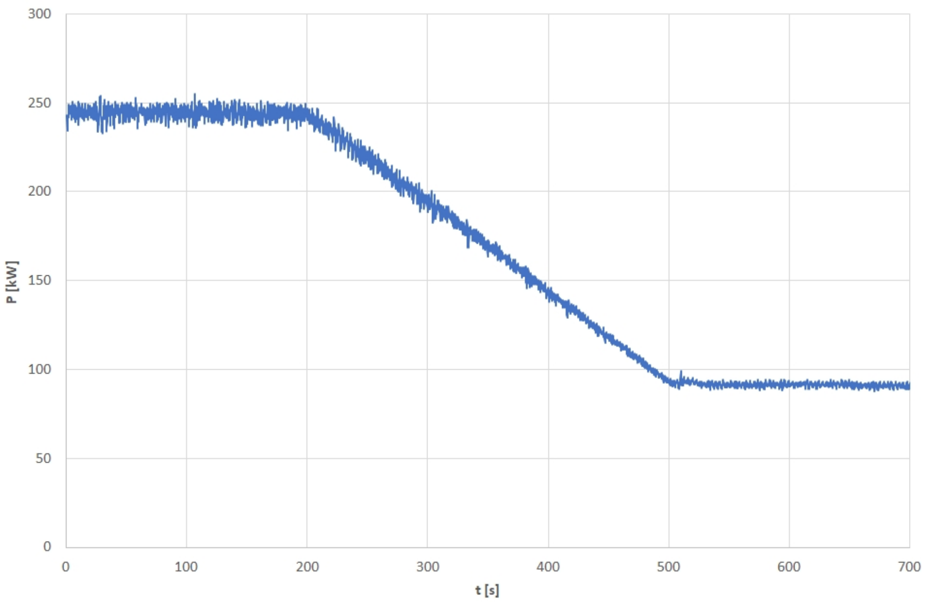

Fig. 6. A diagram illustrating the regulation of active power by the logic interface up to 40% of rated power

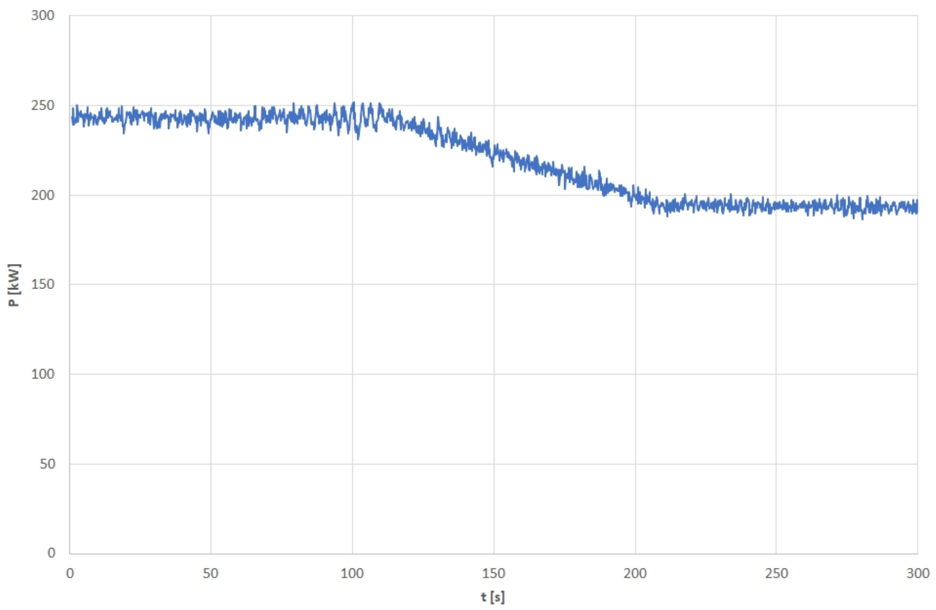

Fig. 7. A diagram illustrating the regulation of active power through the logic interface to 80% of rated power

5. Conclusions

The KOMAG institute's activities under the provisions of the Commission Regulation (EU) 2016/631 of April 14, 2016, establishing a network code on requirements for the connection of generating units to the grid (NC RfG) have led to the fact that producers of generating units can have them subjected to the necessary testing and certification at a national unit offering its services under the accreditation of the Polish Centre for Accreditation. This also applies to CHP units, the use of which is growing steadily, due to the significantly higher efficiency of heat and electricity generation during the same technological process, as well as the possibility of using biogas and biofuels.

The experience gained during the testing of CHP units, selected results of which are presented in this article, confirm the desirability of subjecting these products to testing and certification. These activities reassure manufacturers and power system operators about the characteristics of power generating units offered on the market, including CHP units.

References

[1] Reduction of greenhouse gas emissions: European Parliament. Article dated 31.10.2023. 20180305STO99003

[2] Modern district heating. Cogeneration: more energy without increased emissions. https://nowoczesnecieplownictwo.pl/kogeneracja/ [accessed: 31.10.2023]

[3] Commision Regulation (EU) 2016/631 of 14 April 2016 establishing a network code on requirements for grid connection of generators - Official Journal of the European Union 27.4.2016 L 112/4

[4] Decision of the President of the Energy Regulatory Office DRE.WOSE.7128.184.3.2018.ZJ dated July 16, 2018, approved by the President of the Energy Regulatory Office (ERO) https://www.pse.pl/documents/20182/31216853/20180806_decyzja_ure/717e22be-85b2-4aa3-b006-c365ae577f05?safeargs=646f776e6c6f61643d74727565 [accessed: 31.10.2023]

[5] Requirements and procedures for the use of certificates in the process of connection of power generating modules to power grids, version 1.2 effective from 21.04.2021. - A study by the Polish Power Transmission and Distribution Association

[6] General Application Requirements resulting from the Commission Regulation (EU) 2016/631 of April 14, 2016 establishing a network code on requirements for grid connection of generators - approved by the

decision of the President of the Energy Regulatory Authority DRE.WOSE.7128.550.2.2018.ZJ dated 2 January, 2019
https://www.pse.pl/documents/20182/31216853/20190102_decyzja_wymogi_RfG.pdf/1edc511f-14f3-4280-aaba-f6d9cf36c8f6 [accessed: 31.10.2023]

[7] Polish Standard PN-EN 50549-1:2019-02 Requirements for generating plants to be connected in parallel with distribution networks - Part 1: Connection to a LV distribution network - Generating plants up to and including Type B

[8] http://ptpiree.pl/documents/opracowania/kodeksy_sieci/lista/2023-10-31-wykaz-urzadzen-akceptowanych-po-01.05.2022.pdf [accessed: 31.10.2023]

Publisher: **KOMAG Institute of Mining Technology, Poland**

https://doi.org/10.32056/KOMAG2023.4.3

Modernization of the VSVEM-1140 electro-mechatronic system for testing the asynchronous motors

Received: 28.12.2023

Accepted: 24.01.2024

Published online: 30.01.2024

Author's affiliations and addresses:

[1] Dnipro University of Technology, av. Dmytra Yavornytskoho, 19, 49005, Dnipro, Ukraine

*** Correspondence:**

e-mail: beshtaa@nmu.one

tel.: +38 0672578962

Oleksandr BESHTA, senior [1*], Serhii KHUDOLII [1], Roman DJUR [1], Illia PELTEK [1]

Abstract:

The article is devoted to the description of practical experience in testing the alternating current electric machines. The results of combining the capabilities of digital systems for collecting and processing information with a powerful electromechanical system are presented. It is the combination of two systems of different purposes that enables creating the state-of-the art diagnostic installations combined into one electro-mechatronic system. Practical results of electric machine tests contain clear explanations of fundamental principles and provide a comprehensive assessment of the condition of electric machines. They use methods of direct charging the electric machines with the possibility of recuperation of electric energy during tests. Thermal state of electrical machine nodes is monitored using the thermal forecasting technologies. Both the methods for various types of tests and means for their implementation are described in detail. This article is intended for engineers involved in designing, manufacturing and testing the electric machines.

Keywords: testing and charging stations, high-voltage alternating current electric machines, energy recovery in braking modes, electro-mechatronic system, thermal diagnostics of electric machines

1. Introduction

According to regulatory documents, every manufactured electric machine must undergo control tests, the main one - a heating test on a special stand, where its load is assumed to be in the nominal mode.

Different methods are permissible for charging the asynchronous motors when testing them regarding warming up; the simplest of which are various brakes (pad, tape, etc.), as well as load by a generator operating on a rheostat [1-3]. When using these methods, the energy spent during the tests is irretrievably lost.

There are the warming-up test schemes in which most of the energy used is returned to the grid [4-8]. Naturally, these schemes are better, but the test devices become more complicated and expensive, therefore, in the test schemes of electrical repair companies, such installations are rarely used.

When it became necessary to create a test station to improve the quality of repaired mine electric motors for driving coal harvesters and increase the period of their trouble-free operation, it was proposed to create a new complex test station, on the basis of which it is possible to conduct the entire set of tests defined by standards [8-10].

To increase the efficiency of the test station and save electricity during tests, this station implemented a load mode with a reverse operation scheme using an asynchronous generator controlled by the power grid. In addition to testing electric motors for warming up, loading them in the nominal mode, state-of-the-art electronic devices were developed and manufactured for the test station ion all the necessary stages of testing, which are provided for by current national and international standards, i.e.:

1. TestEM FR "TestFron" - a device for testing the electrical strength of the body insulation of rotating electric machines with a voltage of up to 1140 V relative to the body of the machine and between the windings, and burning of the body insulation with alternating or constant voltage (≈5/=7.5 kV);
2. TestEM Tesel-5 - a device for testing the insulation of bulk windings (5 kV, 6.6 kHz);
3. TestEM Sentor SR3 - a device for testing the insulation of rigid sections (8-16-26 kV, 50 Hz);
4. TestEM AN1 Actron - a device for testing the steel - to determine specific loss of steel;
5. TestEM IR Intor - rotor tester - a device for detecting malfunctions and damage in rotors with short-circuited rods during their manufacture, repair or preventive inspection without limiting their power;
6. TestEM ST Shast - a device for monitoring the insulation of the sheets of active steel;
7. Vibration spectrum analyser 795M107Vi;
8. Thermal imager Flir E8-XT.

The test program, methods and scope of tests, methods and devices for measuring electrical and non-electrical quantities, and methods for determining the nominal parameters of rotating AC electric machines meet the requirements of current national and European standards [9-12].

A set of devices for post-operational tests, together with a stand for loading electric motors and the necessary power and measuring equipment, operating in automatic mode under the control of a microprocessor system, made up, as a result, the first version of the complex electro-mechatronic system VSVEM-1140.

This version of VSVEM-1140 enabled control tests of mine explosion-proof asynchronous three-phase electric motors of type SG7W 490L-4 manufactured by Dombrovsky Plant of Electric Machines Damel (Poland) with power of 220 and 250 kW. When testing these electric motors with a load power of the test machine of 220 kW, about 195 kW of electrical energy was returned to the grid.

Fig. 1 shows a screenshot of the SCADA system screen, which displays the active power of the drive motor (blue colour - average power of about 200 kW) and the motor under test (red colour - average power of about 175 kW). In this case, the efficiency of VSVEM-1140 is approximately 87.5%.

Publisher: **KOMAG Institute of Mining Technology, Poland**

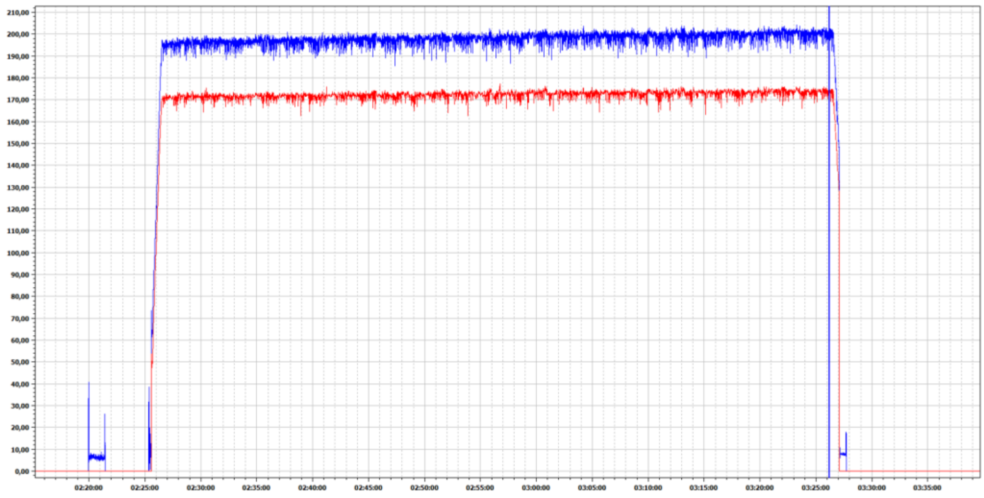

Fig. 1. Active power curves of motors during testing

Prior to the commissioning of VSVEM-1140 in the mines, due to the short life of the electric motors driving the coal harvesters and the need for their frequent replacement, it was not possible to form a sufficient reserve of serviceable repaired engines, which interfered with the rhythmic work and threatened to disrupt the production program. The operation of VSVEM-1140 has shown its high efficiency - the life span of repaired electric motors that have successfully passed thermal tests has increased several times - from several days and weeks to many months.

After analysing the results of the 1.5-year operation of VSVEM-1140 system, it was decided to modernize it to enable testing the mine explosion-proof asynchronous three-phase electric motors with a power of up to 315 kW, voltage of 1140 V and a rotation frequency of 500, 1000 and 1500 rpm. This second version of the electromechatronic system has got the name VSVEM-1140 500-1500.

In the new VSVEM-1140 500-1500 system, all the functions of the first version have been preserved with minor additions, which mainly concern the display of service information (another screen has been added) and the algorithm for calculating the efficiency and torque of the tested electric motor. The main difference of the modernized version is the expansion of the speed range of the motors tested while maintaining the maximum power up to 315 kW. For this purpose, the drive motor 2SGS-355L4, 315 kW, 1140 V, 1500 rpm of the electromechatronic system is rewound to an operating voltage of 380 V at a speed of 1500 rpm to the maximum possible power in the 2SGS-355L4 enclosure, but not lower than 315 kW.

Thus, the modernized electromechatronic system VSVEM-1140 500-1500 is designed for testing the motors with a power of up to 315 kW, a nominal voltage of 1140 V and a different number of poles corresponding to type series 4, 6, 12.

There is a problem of determining the nomenclature of asynchronous motors that can be tested in a long-term load mode by the VSVEM-1140 500-1500 system in the speed range of 500...1500 rpm with a power of up to 315 kW and voltage of 380 V.

The main components of the station are presented in Fig. 2.

Publisher: **KOMAG Institute of Mining Technology, Poland**

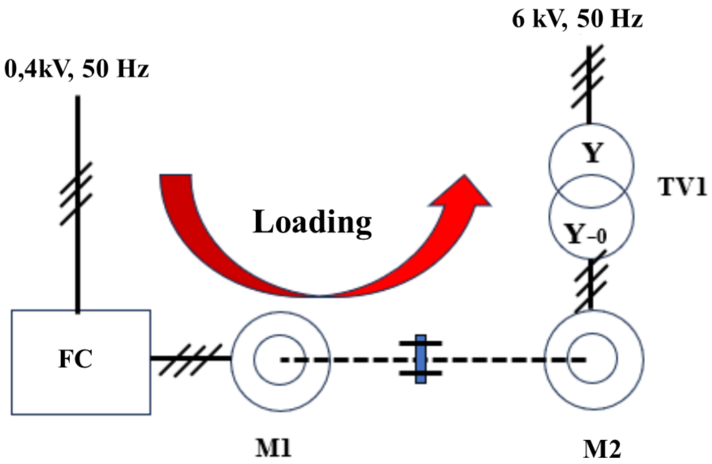

Fig. 2 VSVEM-1140 test station: FC – frequency converter; M1 – loading machine; M2 – tested machine; TV1 - transformer

The load device is represented by the FC frequency converter [13] and the M_1 motor, which brings the test machine into regenerative braking mode. Technical data of the frequency converter are presented in Table 1.

To reduce electricity consumption, the load on the test motors is applied in the generator mode of electricity recovery to the grid. For this, the machine $M_{(2,i)}$ with a supply voltage of 1140 V, different power up to 315 kW and different ideal idle speeds of 500 rpm, 1000 rpm and 1500 rpm are connected via a coupling to the electric motor M_1, and it accelerates to the idle speed $\omega_{(x,i)}$ and then to the ideal idle speed of the corresponding electric machine $M_{(2,i)}$. After that, the machine $M_{(2,i)}$ is connected to the 6kV, 50Hz network through the transformer TV1. For machines of the $M_{(2,i)}$ type, acceleration from the idle speed $\omega_{(x,i)}$ to the ideal idle speed $\omega_{(0,i)}$ occurs already at a frequency of the supply voltage of the motor M1 greater than 50Hz. Next, by increasing the speed of the motor M1, the machine $M_{(2,i)}$ enters the regenerative braking mode and accelerates to the speed $\omega_{(g,i)}$, when the torque of the machine $M_{(2,i)}$ will be equal to the nominal $M_{(n,i)}$ (Fig. 3).

Table 1. Frequency converter FCh5-S0-630/380/50-O70-V00-UHL4

Nominal parameters	Value
Nominal current, A	630
Nominal output voltage, V	380
Nominal output power, kVA	415
Power factor, no less	0,90
Efficiency coefficient, not less, %	95,0
The range of three-phase output voltage change, V	0-380
The range of output voltage frequency change, Hz	0-200

In addition to the standard protection systems of the frequency converter, the control and protection system of the VSVEM-1140 test station additionally includes hardware and software protections, such as protection of the load and test motors by current, power, overheating, temperature, flow and pressure of the coolant, etc.

Publisher: **KOMAG Institute of Mining Technology, Poland**

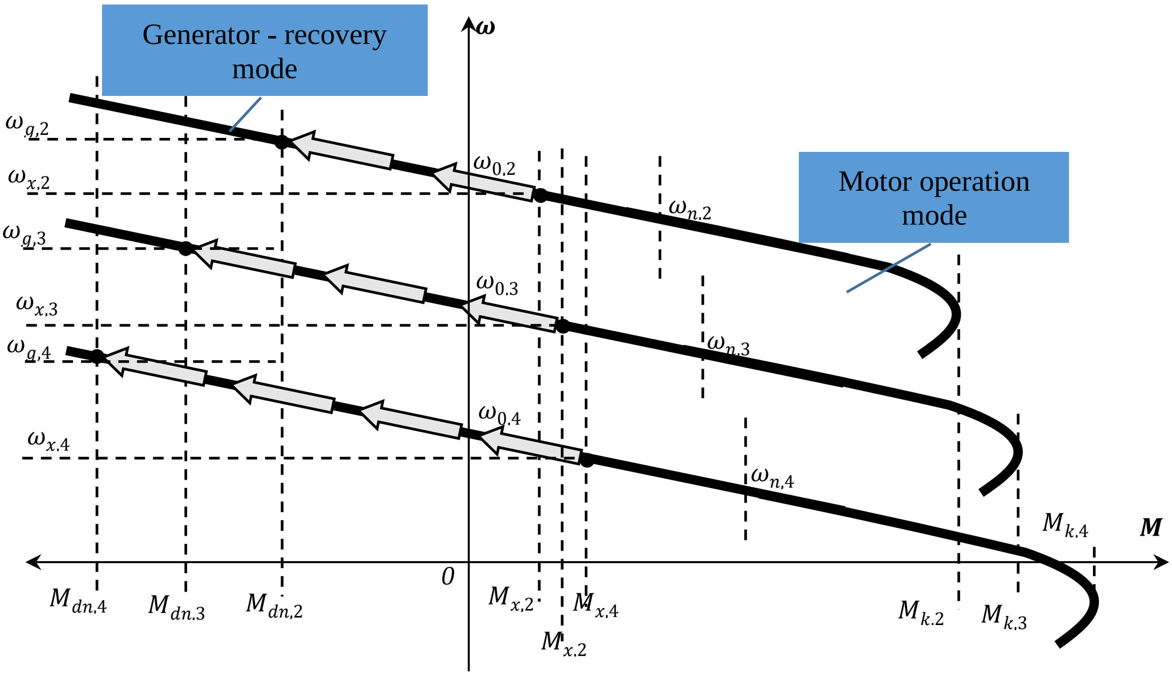

Fig. 3. Mechanical characteristics of tested machines:
i=2 – 1500 rpm; i=3 – 1000 rpm; i=4 – 500 rpm

2. Materials and Methods

The mechanical characteristics of the test machines (Fig. 2) are determined by the simplified Kloss formula in the case when the active resistance of the stator windings of electric machines can be neglected [4, 6, 14]:

$$M_{d,i} = \frac{2M_{k,i}}{S_i/S_{k,i}+S_{k,i}/S_i}, \tag{1}$$

where $M_{(d,i)}$ is the moment on the shaft of the ith tested electric machine, Nm; S_i – sliding; $M_{k,i}$ – critical torque, Nm; $S_{(k,i)}$ – critical slip.

$$M_{k,i} = \lambda_i M_{dn,i}\ , \tag{2}$$

where $M_{(dn,i)}$ is the nominal torque on the shaft of the ith tested electric machine, Nm; λ_i is its ability to overload.

$$S_i = \left(\frac{\omega_{0,i}-\omega_i}{\omega_{0,i}}\right), \tag{3}$$

where $\omega_{(0,i)}$ is the ideal idling speed, rad/sec.; ω_i is the current angular speed of the ith test electric machine.

For the generator load mode, from formula (3) we have the corresponding slip value.

$$S_{g,i} = \left(\frac{\omega_{g,i}-\omega_{0,i}}{\omega_{0,i}}\right). \tag{4}$$

If we consider the working part of the mechanical characteristics of the tested electric machine, where is its nominal working point (corresponding to the points $\omega_{n,2}$, $\omega_{n,3}$, $\omega_{n,4}$ in Fig. 2, that is, when $S_i \ll S_{k,i}$, then equation (1) is further simplified

$$M_{d,i} = \frac{2M_{k,i}S_i}{S_{k,i}}. \tag{5}$$

From the formula (5) we have the nominal mode of the testing machine

$$S_{k,i} = 2S_{n,i}\left(\frac{M_{k,i}}{M_{dn,i}}\right) = 2\lambda_i S_{n,i}. \tag{6}$$

Considering that in the recovery mode there should be a nominal load torque $M_{(dn,i)}$ on the tested machine during sliding $S_{(g,i)}$, from the formula (5) we get:

$$M_{dn,i} = \frac{2M_{k,i}S_{g,i}}{S_{k,i}}, \tag{7}$$

$$M_{dn,i} = P_{dn,i}/\omega_{n,i}, \tag{8}$$

where $P_{dn,i}$ – nominal power of the tested motor, W.

Substituting formulas (2), (4) and (6) into formula (7), we have

$$\omega_{g,i} = 2\omega_{0,i} - \omega_{n,i}. \tag{9}$$

Realization of the torque $M_{(dn,i)}$ of the tested machine must be secured by the motor M_1. To do this, it will create an active torque $M_{(dn,i)}$ at speed of $\omega_{(g,i)}$, that is, it will realize the following power:

$$P_{d1,i} = M_{dn,i}\omega_{g,i}. \tag{10}$$

To ensure this power, the motor M_1 receives energy from the FC frequency converter with an efficiency of η_1, i.e.

$$P_{d1,i} = \sqrt{3}V_1 I_{1,i} cos\varphi_1 \eta_1, \tag{11}$$

where V_1, $\cos\varphi_1$, η_1 - linear supply voltage, power factor and efficiency of the motor M_1, respectively; $I_{(1,i)}$ is the linear current of the motor M_1, which corresponds to the loading moment $M_{(d1,i)}$.

Thus, from the formulas (9), (10) and (11), the current of the loading motor M_1 is determined:

$$I_{1,i} = \frac{M_{dn,i}\omega_{g,i}}{\sqrt{3}V_1 cos\varphi_1 \eta_1}, \tag{12}$$

where $\omega_{(g,i)}$ is found according to formula (9), $M_{(dn,i)}$ is according to formula (8), and the parameters $P_{(dn,i)}$, $\omega_{(0,i)}$, $\omega_{(n,i)}$ are from the catalogue data of tested motors; V_1, $\cos\varphi_1$, η_1 - M_1 motor parameters.

The recovery mode current $I_{(g,i)}$ of the tested machine is determined for the power according to formula (10), but taking into account the efficiency factor η_i of this machine in generator mode

$$I_{g,i} = \frac{M_{dn,i}\omega_{g,i}\eta_i}{\sqrt{3}V_{n,i} cos\varphi_i}, \tag{13}$$

where $V_{n,i}$,$\cos\varphi_i$,η_i are respectively the rated voltage, power factor and efficiency of the tested motor M_i.

3. Results

According to the above formulas, calculations were made for the motors of different power and speed. The results are presented in Table 2.

Columns 1...10 of Table 2 present catalogue data of electric motors. As a result of using the suggested method, the load currents $I_{1,i}$ of the motor M_1 in the VSVEM-1140 test station and the possible long-term load current $I_{g,i}$ of the motor being tested were obtained.

Since it is planned to use a motor rewound from 1140 V to 380 V as the drive motor M_1, the assessment of its loading current is important from the point of view of overload due to a significant increase in stator currents. After rewinding, the drive motor must have a nominal current proportionally increased in relation to the decrease in the nominal voltage, i.e. assuming the power, efficiency and power factor are maintained at the previous levels, an increase in the current of the stator windings of the drive motor M_1 to the level of 829 A should be expected. From column 14 of Table 2 we can see that the currents of the driving motor do not exceed 588.4 A.

4. Conclusions

Testing the possibility of maintaining the long-term current load of the motors presented in Table 2, using the VSVEM-1140 electro-mechatronic system with a drive motor after rewinding from a voltage of 1140 V to a voltage of 380 V, showed the following:

- motors with a rated power of up to 315 kW, inclusive, with any speed in the range of 500...1500 rpm can be tested at the VSVEM-1140 station with the rated load for these motors in a long-term mode.
- the ratio between the currents of the motor M_1 and the tested machine M_i varies within 2.1...3.5;
- the range of currents 2.1...2.5 is typical for motors with a speed of 500 rpm, and the range 3.2...3.5 - for motors with a speed of 1000 rpm and 1500 rpm, i.e. an increase in speed of the driving motor causes an increase in its current load and losses;
- acceleration of the tested motor in the recovery mode should be carried out with monitoring the current acceleration of the M_1 motor.

Thus, the VSVEM-1140 500-1500 electro-mechatronic system can be used to expand the range of the motors with power up to 315 kW in the speed range of 500...1500 rpm to test their load power in long-term operation.

Table 2. The results of calculating the load on the M_1 engine when testing engines with a voltage of 1140 V

$P_{dn,i}$ kW	n_0 r/min	$V_{n,i}$ V	$I_{n,i}$ A	$S_{n,i}$ %	η_i	$cos\varphi_i$	$\omega_{n,i}$ rad/s	$\omega_{0,i}$ rad/s	$\omega_{g,i}$ rad/s	$M_{dn,i}$ Nm	$I_{g,i}$ A	$I_{1,i}$ A
1	2	3	4	5	6	7	8	9	10	11	12	13
7,5	1500	1140	5	3.4	0.875	0.86	151.7	157.0	162.3	49.5	4.1	14.7
11			7.2	3.9	0.875	0.87	150.9	157.0	163.1	72.9	6.1	21.8
15			10.1	2.5	0.9	0.84	153.1	157.0	160.9	98.0	8.6	28.9
18,5			12.3	2.6	0.95	0.85	152.9	157.0	161.1	121.0	11.0	35.7
22			14	2.4	0.891	0.83	153.2	157.0	160.8	143.6	12.5	42.3
30			18.7	2.4	0.9	0.85	153.2	157.0	160.8	195.8	16.9	57.6
75			49	1	0.922	0.89	155.4	157.0	158.6	482.5	40.1	140.1
90			58	1	0.925	0.9	155.4	157.0	158.6	579.0	47.8	168.1
45	1000		29	1.5	0.916	0.87	103.1	104.7	106.2	436.5	24.7	84.9
55			36.3	1.5	0.922	0.87	103.1	104.7	106.2	533.5	30.4	103.8
75			48.1	1.5	0.932	0.86	103.1	104.7	106.2	727.5	42.4	141.5
90			56.3	1.8	0.934	0.87	102.8	104.7	106.6	875.6	50.7	170.8
315			189	1	0.954	0.88	103.6	104.7	105.7	3040.0	176.4	588.4
75	1500		49	1.8	0.922	0.85	154.2	157.0	159.8	486.5	42.7	142.4
110			70.5	1.8	0.93	0.85	154.2	157.0	159.8	713.5	63.2	208.8
132			84.4	1.8	0.932	0.85	154.2	157.0	159.8	856.2	76.0	250.5
160			104.7	1.9	0.933	0.83	154.0	157.0	160.0	1038.8	94.6	304.3
200			130.8	1.4	0.934	0.83	154.8	157.0	159.2	1292.0	117.2	376.6
45	500		57.6	2	0.825	0.48	51.3	52.3	53.4	877.4	40.8	85.8
132	1500		88.6	1.7	0.91	0.83	154.3	157.0	159.7	855.3	75.8	250.0
55	500		67.5	2	0.826	0.5	51.3	52.3	53.4	1072.4	47.9	104.8
160	1500		102.6	1	0.93	0.85	155.4	157.0	158.6	1029.4	90.4	298.9
65	500		76.1	2.1	0.838	0.52	51.2	52.3	53.4	1268.7	55.3	124.1
200	1500		126.5	1.1	0.932	0.86	155.3	157.0	158.7	1288.1	112.2	374.3
85	500		85.5	2.8	0.84	0.6	50.9	52.3	53.8	1671.0	63.7	164.6
250	1500		152.9	2.1	0.931	0.89	153.7	157.0	160.3	1626.5	138.1	477.4

Publisher: **KOMAG Institute of Mining Technology, Poland**

References

[1] Rolf Fischer, Eugen Nolle Elektrische Maschinen: Aufbau, Wirkungsweise und Betriebsverhalten Hardcover – 10 Dec. 2021 ISBN-10: 3446469125, ISBN-13: 978-3446469129

[2] Okubo, Hitoshi & Hayakawa, Naoki & Montanari, Gian. (2008). Technical Development on Partial Discharge Measurement and Electrical Insulation Techniques for Low Voltage Motors Driven by Voltage Inverters. Dielectrics and Electrical Insulation, IEEE Transactions on. 14. 1516 - 1530. 10.1109/TDEI.2007.4401236. https://doi.org/10.1109/TDEI.2007.4401236

[3] Peter Tavner, Li Ran, Christopher Crabtree/ (2020) Condition Monitoring of Rotating Electrical Machines (3rd Edition). Energy Engineering. ISBN-13: 978-1-78561-865-9, Book DOI https://doi.org/: 10.1049/PBPO145E

[4] Elektrische Maschinen und Antriebe: Lehrbuch / E. Nolle, A. Beshta. – D.: Nationale Bergbauuniversität, 2013. – 232 p. ISBN 978 – 966 – 350 – 418 – 6.

[5] Deshpande, M. V. . Design and Testing of Electrical Machines. Prentice-Hall Of India Pvt. Limited. (2010) ISBN:9788120336452, 8120336453

[6] Cooling of Rotating Electrical Machines Fundamentals, modelling, testing and design. David Staton, Eddie Chong, Stephen Pickering, Aldo Boglietti. – 268 p. - ISBN-13: 978-1-78561-351-7. 2022

[7] H. Henao et al., "Trends in Fault Diagnosis for Electrical Machines: A Review of Diagnostic Techniques," in IEEE Industrial Electronics Magazine, vol. 8, no. 2, pp. 31-42, June 2014, https://doi.org/10.1109/MIE.2013.2287651.

[8] Dineva, A., Mosavi, A., Gyimesi, M., Vajda, I., Nabipour, N., & Rabczuk, T. (2019). Fault diagnosis of rotating electrical machines using multi-label classification. Applied Sciences, 9(23), 5086. https://doi.org/10.3390/app9235086

[9] IEC 60034-1:2017 Rotating electrical machines – Part 1: Rating and performance

[10] IEC 60034-2-1:2014 Rotating electrical machines – Part 2-1: Standard methods for determining losses and efficiency from tests (excluding machines for vehicles)

[11] Molina Llorente, R. Practical Control of AC Machine. In: Practical Control of Electric Machines. Advances in Industrial Control. Springer, Cham.2020 - https://doi.org/10.1007/978-3-030-34758-1_

[12] Toliyat, H. A., Nandi, S., Choi, S., & Meshgin-Kelk, H. (2012). Electric machines: modeling, condition monitoring, and fault diagnosis. CRC press. ISBN:0849370272, 9780849370274

[13] https://pcomplex.ua/ru/products_pt/pch5-d0-100-380-50-d40-v01-ukhl4-2/ [accessed: 28.11.2023]

[14] Колб Ант. А. Теорія електроприводу: Навчальний посібник [Текст] / Колб Ант.А., Колб А.А. – Д.: Національний гірничий університет, 2006 – 511 с *(Kolb Ant. A. Electric drive theory: Study guide [Text] / Kolb Ant.A., Kolb A.A. - D.: National Mining University, 2006 - 511 p)*

e-ISSN 2719-3306 Mining Machines, 2023, Vol. 41 Issue 4, pp. 248-260

https://doi.org/10.32056/KOMAG2023.4.4

Concept of a technological system for manufacturing the composite products based on impregnated wood waste

Received: 21.12.2023

Accepted: 22.01.2024

Published online: 30.01.2024

Author's affiliations and addresses:

[1] KOMAG Institute of Mining Technology, Pszczyńska 37, 44-101 Gliwice, Poland

*** Correspondence:**
e-mail: rbaron@komag.eu

Rafał BARON [1*], Paweł FRIEBE [1], Daniel KOWOL [1], Piotr MATUSIAK [1]

Abstract:

The article presents the results of the research work, which included a qualitative and quantitative analysis of the selected wooden wastes intended for manufacturing the composite materials. Additionally, the existing solutions related to the processing of wooden waste from power poles and railway sleepers were analysed. In the context of the analysis, the focus was on the methods for removing carcinogenic substances used for preserving the telecommunications poles, power poles and railway sleepers, with the aim of obtaining the safe end product. On this basis, the concept of a technological system for recycling the mentioned wastes has been developed. The recycling process involves reprocessing them and using as components of the composite materials.

Keywords: impregnated wood wastes, power poles, railway sleepers, composites

1. Introduction

For over 60 years, the European industry has produced impregnated wooden poles in accordance with industry guidelines and national standards as well as specifications of the Wood European Institute (WEI). These standards are changing gradually, as knowledge about the harmfulness of the chemicals used for impregnation increases. These regulations in the past allowed the use of wood preservatives/impregnators containing hazardous chemicals. Three main chemical wood preservatives are as follows:

- creosote,
- pentachlorophenol,
- arsenate (copper-chromium-arsenic, i.e. CCA),
- copper naphthenate (alternative agent) [1, 2].

In 2001, the European Union severely restricted the sale and use of tar. In January 2003, the European Union announced a ban on all industrial uses of CCA, except for a limited number of special cases. Creosote was phased out in Poland temporarily in 2013, and finally from April 2018. Restrictions related to the use of chemical wood preservatives are the subject of ongoing discussion [2, 3].

FRP composite materials are materials made of a polymer matrix reinforced with fibres. The most commonly used fibres are glass, carbon, aramid, basalt and mixed fibres, e.g. basalt-carbon. Epoxy, polyester or vinyl ester resins are most often used as matrices [4, 5].

Due to a number of advantages, including: low density, high anti-corrosion and chemical resistance, as well as high strength, stiffness and durability, the above-mentioned. materials have found wide application. Unfortunately, the main advantages of composites such as durability are at the same time their disadvantages. Even though various methods of processing the composite materials are known (pyrolysis, solvolysis, mechanical methods). Although various methods of processing the composite materials are known, only a small amount of waste is recycled [6, 7].

1.1. Impregnated wood in railway sleepers

Impregnation is a technology used in manufacture of railway sleepers (Fig. 1) to increase the durability and resistance of wood to weather conditions, as well as to protect it against biological organisms. Creosote is one of the frequently used impregnating agents, but other chemicals are also used, such as petroleum oils and heavy metal salts [8, 9].

Fig. 1. Impregnated wood in railway sleepers [10]

Based on data from 2018, the number of railway sleepers intended for recycling or neutralisation in Poland is over 20 million pieces. With an average weight of one sleeper of approximately 80 kg, it gives 1,600,000 Mg of impregnated wood waste [11].

1.2. Impregnated wood in poles

In Poland, impregnated poles (Fig. 2) are commonly used in various sectors of industry, such as power, telecommunication, in road infrastructure, etc. Impregnation of poles is intended to increase their durability and resistance to weather conditions and insects, fungi and other factors that may cause wood degradation [12].

Fig. 2. Impregnated telecommunication pole [13]

Orange Polska S.A. as well as Tauron Polska Energia S.A. have about 2 million pieces of wooden poles impregnated with carcinogenic substances. Due to their toxicity, they should be replaced as soon as possible. The technology suggested further will allow for elimination of the above-mentioned hazard [14].

Both wooden and composite components is the waste which, from the point of view of the circular economy model and should be used as a raw material in subsequent manufacturing stages.

Division of electric, telephone, street and parking (lighting) poles in the world, depending on the type of material used, is presented in Table 1 [15].

Table 1. Division of poles in the world, depending on the type of material used [15]

Place	Pole material				
	Wood	Concrete	Steel	Composite	Total
	Number of pieces [mil.]				
Europe	133	48	77	4	262
CIS	78	34	18	1	130
Near East	2	13	34	0	50
North Africa	22	9	10	1	42
Sub-Saharan Africa	43	6	8	0	58

Publisher: **KOMAG Institute of Mining Technology, Poland**

Place	Pole material				
	Wood	Concrete	Steel	Composite	Total
	Number of pieces [mil.]				
Asia-Pacific	157	421	125	8	710
Latin America	96	28	39	2	165
North America	202	20	51	4	277
Total	732	579	362	21	1,694

Based on the data presented above, it can be concluded that there are a very large number of wooden poles in the world that will be recycled in the future. Table 2 shows the total weight of wooden poles, assuming a pole weight of 160 kg [15].

Table 2. Division of wooden poles in the world, with estimation of their weight [15]

Place	Wooden poles	
	Number of pieces [mil.]	Weight [Mg]
Europe	133	21 280 000
CIS	78	12 480 000
Near East	2	320 000
North Africa	22	3 520 000
Sub-Saharan Africa	43	6 880 000
Asia-Pacific	157	25 120 000
Latin America	96	15 360 000
North America	202	32 320 000
Total	732	117 280 000

In Poland there is 2 mil. poles with weight of 320 000 Mg [14].

Therefore, the aim of the task is to develop a concept of technology for manufacturing the composite products from the waste wood, e.g. from the railway sleepers and the power poles. The developed concept will be used, in the next stages, to produce structural components for the power industry, e.g.: state-of-the-art composite poles.

2. Materials and Methods

The most popular method of "utilizing" impregnated wood from power poles or railway sleepers is to store and burn them.

The disposal of old wooden components of power and transport infrastructure, such as power poles and railway sleepers are important from an ecological, social and safety perspective. Old wooden components are aging, which may lead to weakening of the wood structure, to its damage caused by weather conditions as well as by insects and fungi. This may contribute to the loss of stability of the power pole and, consequently, breakage of electrical cables. Moreover, these components are covered with carcinogenic substances that are harmful to humans and the environment. To minimize the negative impact of old wooden poles on the environment and society, it is necessary to develop appropriate disposal processes.

Publisher: **KOMAG Institute of Mining Technology, Poland**

Disassembly is the first stage of disposal. Used wooden power poles are removed from their original installation place. This process requires special equipment and technical knowledge to avoid damage and hazards to workers and the environment. Disassembly can be manual or using the machines such as cranes or special vehicles. It is important that this process follows the safety regulations and industry standards.

Then, the next important step is transporting the wooden poles to the processing site. Timber can be transported by truck or other means of transport.

Wood that cannot be recycled or reused is burned to produce heat or electricity. The process is becoming increasingly popular in some regions as a way to extract energy from materials that would otherwise end up in a landfill.

Disposal in a controlled landfill is another option that requires monitoring and management to avoid environmental contamination. According to the currently applicable regulations, disabled power poles can be stored for up to 3 years. Then they must be processed or sold [16].

There are the following alternative approaches to removing the hazardous substances from wood:

- Mechanical removal: This is one of the basic methods. It involves manual grinding, planeing or scraping of the wood surface to remove the contaminated layer.
- Sandblasting: This is a more advanced method of mechanically removing substances from wood. It involves applying a stream of sand grains under pressure to the wood surface, which helps to remove contaminants more effectively.
- Chemical removal: Special chemicals are used that dissolve or soften chemicals present on the wood surface, such as sealers or paints. Then the impurities are removed mechanically.
- Thermal stripping: This involves heating the wood to a high temperature, which can help evaporate or break down chemicals. This is particularly effective in removing certain sealers.
- Ozonation: Ozone is a strong oxidant and can be used to remove chemicals from wood. This process involves the impact of ozone on saturated wood, which reacts with pollutants, leading to their decomposition.
- Microwave stripping: This method uses microwave waves to heat chemicals present in the wood, which can help break them down.
- Enzymatic method: Uses enzymes that have the ability to break down chemicals. This is a relatively new technology that is becoming more and more popular.
- Biodegradation: Uses microorganisms such as bacteria or fungi to naturally break down chemicals [17].

All stages of the disposal of wooden power poles must be in accordance with the applicable regulations and standards regarding environmental protection, health and safety.

To sum up, the disposal of old wooden power poles or railway sleepers is a complex process that aims to minimize the negative impact on the environment and society. Appropriate disassemble, transport, processing, recycling and energy recovery are crucial for the effective use of wood after its original function has ended. A deep knowledge of local regulations and the use of sustainable disposal methods are the foundations of this process, contributing to better protection of our environment.

Research work in Poland and abroad in the scope of a discussed problem

Recycling of the impregnated wood is a complex task due to the presence of chemicals used during the impregnation process.

Therefore, wood recyclers must use special methods to safely remove or neutralize these substances. In only a few regions and countries there are the companies specializing in recycling the impregnated wood. However, the activities of this type of companies are much less common than in the case of recycling the typical wood [18].

Publisher: **KOMAG Institute of Mining Technology, Poland**

Engineers from Belgium and Finland have introduced innovative solutions that are alternative to the traditional waste storage. The solution uses reactors enabling gasification and simultaneous neutralization of poisonous hydrocarbons. Moreover, one of the promising technologies for creosote neutralization is the biodegradation method, which is based on the biological decomposition of oily substances by the specially selected microorganisms. This innovative method is not only safe for the environment, but also eliminates waste, which makes it relatively economical [19].

In the biodegradation method, there are the following key elements of removing creosote from wood:

– Selected microorganisms: The creosote biodegradation process uses microorganisms capable of decomposing chemicals contained in creosote. These microorganisms are carefully selected and adapted to the conditions in which the process will be carried out.
– Biological degradation: Microorganisms used in biodegradation have the ability to metabolize poisonous chemicals contained in creosote. As a result of this process, creosote is transformed into more stable, less toxic compounds, what means its neutralization.
– Optimal conditions: For the biodegradation process to be effective, it is necessary to maintain optimal conditions such as temperature, pH, humidity and nutrient availability. Microorganisms function most effectively under specific conditions that must be controlled during the process.
– Monitoring and control: The biodegradation process requires monitoring and control to ensure effectiveness and environmental safety. Parameters such as chemical composition and amount of creosote before and after the process are monitored and process conditions are adjusted as necessary [20, 21].

Tests also included the use of lactic acid bacteria *Lactobacillus bulgaricus* and *Streptococcus thermophilus*, allowing for the extraction of up to 93% of copper, 86.5% of chromium and 97.8% of arsenic after 8 days of fermentation (Fig. 3) [20].

Fig. 3. Use of lactic acid bacteria for the degradation of wood preservatives. Milled treated and untreated wood sample before or after bioprocessing treatment [20]

Fungi also have the ability to degrade molecules contained in preservatives such as creosote. The use of fungi has shown good results, especially when this method is combined with a citric acid. Nevertheless, positive results have been obtained on a laboratory scale, but the physiological mechanisms implemented by microorganisms are still poorly understood [20].

It is worth emphasizing that the effectiveness of the biodegradation method may depend on many factors, including the chemical composition of creosote, the type of microorganisms used in the process and the process conditions. Disadvantage of the method is the need to adapt it to a specific case and the proper biodegradation time [20, 21].

Publisher: **KOMAG Institute of Mining Technology, Poland**

3. Results

Based on the analysis of the literature and available information on the characteristics of impregnated wood, the initial concept of the system for its reuse was developed. The conceptual system for the production of new products from waste wood assumes using the processes from disassembly, through grinding, to obtain a new product (Fig. 4). The rest of the article describes in detail each stage of the conceptual technology for recycling the wood waste. The concept was developed on the example of recycling the power poles.

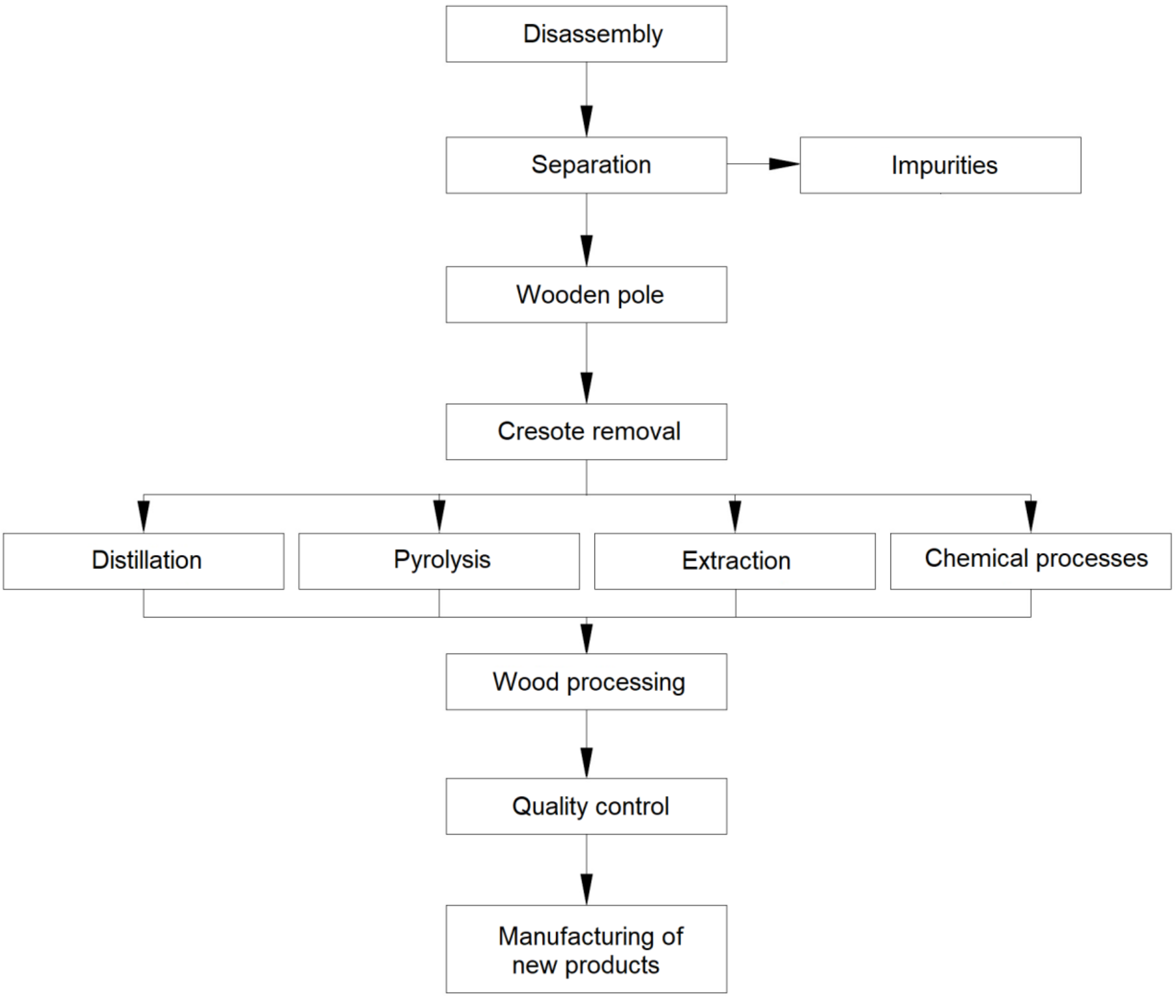

Fig. 4. Conceptual path for manufacturing new products from waste wood

Disassembly:

Power poles are first disassembled from their original location. This process requires special equipment and appropriate safety procedures because crested wood is treated as a hazardous material. Dismantling is carried out using simple construction equipment (saws, ropes, safety elements, etc.). The waste in question is then transported to a dismantling point, where it is subjected to the process of removing any insulating materials, such as wires or cables, that may be attached to them. Alternatively, the process can be expanded to include the use of vibrating screens to remove unwanted elements [22].

Removal of creosote:

Removing the creosote is one of the key steps in recycling impregnated wooden poles. There are various methods that can be used to remove creosote from wood. Future laboratory tests will analyse the most advantageous method for removing the creosote. The methods to analyse are as follows:

– Distillation: distillation process involves heating the wood in special furnaces to evaporate the creosote. The creosote vapor is then condensed and collected, then processed to obtain pure creosote. Distillation is a complicated and energy-intensive process that requires temperature and pressure control.
– Pyrolysis: Pyrolysis is a thermal process in which wood is subjected to high temperatures in limited air access. As a result, creosote and other chemicals break down into simpler compounds. Pyrolysis products, including gas and oil, can be collected and processed.
– Extraction: In this method, creosote is extracted from the wood using chemical solvents. The wood is soaked in an appropriate solvent that removes creosote. The extract is then processed to separate the creosote.
– Chemical processes: There are also chemical processes that can be used to neutralize the creosote contained in the treated wood. Using the proper chemical reagents, creosote can be converted into less toxic compounds.

Processing of wood:

After the creosote is removed, the wood is chipped into smaller pieces and transferred into various wooden products such as boards, beams and fuel. Cutting a pole into boards uses variety of tools, depending on available resources and preferences. Once you have finished cutting, clean the edges of the boards to obtain a clean and smooth finish. Boards prepared in this way are the ready-made commercial product.

The material resulting from cutting and processing, as well as scraps of the pole remaining after cutting the boards, are subjected to additional processes. The sections of the pole are crushed in a branch shredder. In the shredding process, it is important to obtain evenly shredded material with a granulation similar to the waste generated during cutting and processing the boards [23]. The obtained material can be used as fuel, construction material or as input for the production of composite materials.

Quality control:

Once processed, the wood can be subjected to testing and quality control to ensure it has no residual toxic substances and is safe for further use.

Manufacturing the new composite products:

One of the uses of fine wood chips is to make new composite products from them. Manufacturing the composite materials from harvested wood involves combining wood with resin or other polymeric materials to create a durable and versatile product. The manufacturing process assumes implementation of the stages shown in Fig. 5.

The following devices, which forms part of the system for the production of composites from waste wood, has been selected on the basis of our own experience of waste recycling and guidelines provided by the manufacturers of the devices. The estimated capacity of the system is in the range of 400-500 kg per day.

Publisher: **KOMAG Institute of Mining Technology, Poland**

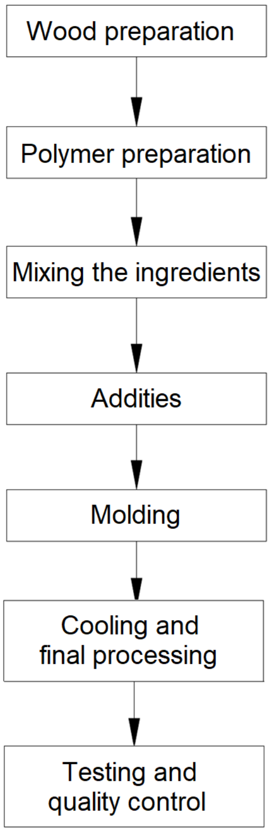

Fig. 5. Manufacturing the new composite products

– Wood preparation - wood crushed into fine fibres, chips or powder is dried in a condensing dryer for wood (Fig. 6) to reduce the water content, which improves the durability of the composite. We suggest the use of a condensation dryer with a capacity of 14m³, which will allow the drying of wood at a temperature of around 70° C.

Fig. 6. Condensing dryer for wood – Eberl TC6WP [24]

– Polymer preparation – the polymer is selected to create the composite matrix. Thermoplastic polymers such as polypropylene, polyethylene or PVC, or thermosetting resins are used for this purpose.

- Mixing the ingredients - wood and polymer are mixed in the required ratio. The process can take place in a wet or dry form (Fig. 7). We propose the use of a mixer with a capacity of 500 kg, equipped with a 3 kW motor.

Fig. 7. Mixer for dry process of multi-component feed mixture - Aluhaus MDS 500 [25]

- Additives - strengthening additives, dyes or antioxidants should be added to the mixture to improve the composite properties.
- Moulding process - the mixture of wood and polymer is formed using various technologies such as extrusion, injection (Fig. 8). In the case of extrusion, the mixture is passed through a forming die to create an extruded mould, which is then cooled and cut to appropriate lengths. The injection process involves injecting a mixture of wood and polymer into a mould, where it hardens under heat and pressure. Once the material has solidified, the mould opens and the finished product is removed. We recommend the use of a plastic injection molding machine with a power of 13 kW and an injection mold size of 480 x 280 mm.

Fig. 8. Plastic injection machine - CAN YANG MACHINERY CY-500C [26]

- Cooling and post-processing - composite products are cooled to obtain their final form. They can be subjected to additional processing, such as cutting, milling or grinding, to obtain the desired shape and surface finish.

– Testing and quality control – the products are tested to check their strength, durability and other important properties. Quality inspections help ensure compliance with industry standards.

The effectiveness of the suggested operations aimed at removing creosote and related to the production of composite products should be confirmed by the laboratory tests.

It should be noted that all stages of processing of creosoted wood must be in accordance with applicable safety and environmental regulations. Employees involved in this process must be properly trained and equipped with appropriate protective equipment. The recycling process can also generate waste such as creosote residue. This waste must be properly disposed in accordance with the regulations for hazardous waste.

4. Discussion

Recycling of impregnated wood has advantages and disadvantages. Below there is analysis of its advantages and disadvantages. A detailed analysis will be possible after testing the effectiveness of creosote removal and manufacture of the composite material.

Advantages:

– Reducing the waste material: Recycling the impregnated wood reduces waste, contributing to sustainable resource management.
– Conservation of resources: Recycling allows wood to be reused, which helps conserve natural resources and reduces deforestation.
– Cost reduction: In the long term, recycling can help reduce costs associated with purchasing new materials and production.
– Environmental protection: Effective recycling can reduce the environmental impact of impregnation chemicals through controlled removal of these substances and minimizing emissions.
– Regulatory compliance: Companies that recycle impregnated wood are typically required to comply with environmental regulations, which contributes to sustainability.

Disadvantages:

– Difficulty in removing chemicals: The recycling process may not be fully effective in removing or neutralizing the chemicals used in impregnation, which poses a potential risk to the environment.
– Technology costs: Advanced technologies necessary for effective recycling of impregnated wood is associated with high costs, which affects the project profitability.
– Lack of standardization of processes: Lack of standardization of recycling processes on a global scale may lead to a lack of uniform quality of recyclates and hinder their subsequent use.
– Potential for toxic emissions: Improper management of the recycling process may lead to accidental emissions of toxic substances into the environment.
– Limited markets: Lack of widespread understanding and acceptance of recycling the impregnated wood may limit markets for recyclates.

5. Conclusions

As part of the research work, wood impregnation and its use in railway and telecommunication infrastructure were analysed in literature. Wood impregnation in telecommunications poles and railway sleepers are mainly used to protect wood against weather conditions, insects, fungi and other pests. Chemical-based impregnations were widely used in Poland. Due to their toxicity, they are carcinogenic, so they should be removed as soon as possible.

Publisher: **KOMAG Institute of Mining Technology, Poland**

Moreover, a concept of a system for recycling the impregnated wood was suggested, including the development of an effective and sustainable process that allows the reuse of this material with minimal impact on the environment. As part of the concept, individual stages of the technology system were developed, allowing for the removal of toxic substances and the production of a new product. The scope of work also included the selection of devices and determining the scope of preliminary laboratory tests. These tests will aim to determine an effective method for removing creosote and verify the assumptions regarding the concept of the production system of composite materials containing impregnated wood waste.

When recycling the impregnated wood, it is crucial to strive for continuous process improvement to minimize disadvantages and maximize advantages. Moreover, development of innovative technologies and increasing public awareness of the benefits of impregnated wood recycling can contribute to improving the situation in this field.

References

[1] Perkitny T.: Działalność zakładu ulepszania drewna w Bydgoszczy, Biuletyn Instytutu Badawczego Leśnictwa, nr.: 3-4, pp.: 366-374, 1951

[2] Cooper, P. “The potential for re-use of preservative-treated utility poles removed from service.” Waste Management & Research, vol. 14, no. 3, 1996, pp. 263–279, https://doi.org/10.1006/wmre.1996.0026.

[3] Rozporządzenie Wykonawcze Komisji (UE) 2022/1950 z dnia 14 października 2022 r. w sprawie odnowienia zatwierdzenia kreozotu jako substancji czynnej przeznaczonej do stosowania w produktach biobójczych należących do grupy produktowej 8 zgodnie z rozporządzeniem Parlamentu Europejskiego i Rady (UE) nr 528/2012

[4] Krzysik A.: Problem impregnowania tarcicy w świetle osiągnięć i doświadczeń szwedzkich, Sylwan, Nr.1, 1976

[5] Nowak J.: Ecological methods of wood impregnation and disposal of wooden waste impregnated with hazardous agents, Science & Technology Days, Białowieża, 2011

[6] Svantesson B.: Material economic aspects of wooden pole fence buildings Examples from a flexible building method, Vol.16 Nr.4, BICCS 23, 2023, 1-12, https://doi.org/10.7577/formakademisk.5421

[7] Anders W. Kjellow, Ole Henriksen, Supercritical wood impregnation, The Journal of Supercritical Fluids, Volume 50, Issue 3, 2009, Pages 297-304, ISSN 0896-8446, https://doi.org/10.1016/j.supflu.2009.06.013.

[8] Fabijański, Mariusz, et al. “Requirements for wood products used in Railway Transport.” WUT Journal of Transportation Engineering, vol. 129, 2020, pp. 27–48, https://doi.org/10.5604/01.3001.0014.2460.

[9] Bouslamti, A, et al. “Why simulate a sample of recycled wood?” Maderas. Ciencia y Tecnología, vol. 14, no. 2, 2012, pp. 145–153, https://doi.org/10.4067/s0718-221x2012000200002.

[10] https://smoglab.pl/podklady-kolejowe-na-opal-kwitnie-sa-toksyczne-rakotworcze-i-szkodliwe-dla-srodowiska/

[11] Wojciechowski A.: Przyjazny dla środowiska recykling podkładów kolejowych, Problemy Kolejnictwa, Zeszyt 181, str.:63-70, ISSN 0552-2145. — 2018

[12] Mączyński D.: Metody zabezpieczania drewna budowlanego i konstrukcyjnego, Ochrona Zabytków 50/4, 372-379, 1997

[13] https://inzynierbudownictwa.pl/rakotworczy-kreozot-na-slupach-telefonicznych-i-energetycznych/ [access 11.12.2023]

[14] https://www.nik.gov.pl/plik/id,25918,vp,28697.pdf [accessed: 11.12.2023]

[15] https://www.eltelnetworks.pl/blog/2022/rodzaje-konstrukcji-wsporczych-linii-elektroenergetycznych/ [accessed: 11.12.2023]

[16] Wasilewski R., Stelmach S.: The problem of waste management of wooden railway sleepers, Archives of waste management and environmental proctection, vol. 16, issue 3, 2014, ISSN 1733-4381

Publisher: **KOMAG Institute of Mining Technology, Poland**

[17] Błaszczyński T., Ksit B., Plich R.: Dawne zabezpieczenia konstrukcyjnych elementów drewnianych wpływające szkodliwie na człowieka i środowisko, Builder Science, 283(2):20-24, 2021, DOI:10.5604/01.3001.0014.6351

[18] https://naukawpolsce.pl/aktualnosci/news%2C30670%2Csposob-biologow-z-uw-na-utylizacje-rakotworczych-podkladow-kolejowych.html [accessed: 11.12.2023]

[19] Leśniewicz M., Kruszelnicka I., Ginter-Kramarczyk D. Problem z zagospodarowaniem drewnianych podkładów kolejowych, Instal, T.10, str.:11-14, 2015

[20] Besserer, Arnaud, et al. "Cascading recycling of Wood Waste: A Review." Polymers, vol. 13, no. 11, 2021, p. 1752, https://doi.org/10.3390/polym13111752

[21] Nguyen, Duy Linh, et al. "Production of wood-based panel from Recycled Wood Resource: A literature review." European Journal of Wood and Wood Products, vol. 81, no. 3, 2023, pp. 557–570, https://doi.org/10.1007/s00107-023-01937-4

[22] Friebe P., Baron R., Sheketa V.: Concept of a CDR resonance screen, Mining Machines, 2022, Vol. 40 Issue 1, pp. 8-18, doi.org/10.32056/KOMAG2022.1.2

[23] Friebe P.: Development of a prototype shredder for WEEE equipped with NdFeB magnets. Mining Machines, 2023, Vol. 41 Issue 2, pp. 143-157. doi.org/10.32056/KOMAG2023.2.6

[24] https://www.eberl-trocknungsanlagen.de/pl/produkty/suszarnia-kontenerowa-air-classic-z-pompa-ciepla.html [accessed: 11.12.2023]

[25] http://www.aluhaus.pl/mieszalniki-do-tworzyw [accessed: 11.12.2023]

[26] https://maszyneria.com/produkt/wtryskarka-can-yang-machinery-cy-500c/ [accessed: 11.12.2023]

Publisher: **KOMAG Institute of Mining Technology, Poland**

https://doi.org/10.32056/KOMAG2023.4.5

Simulating energy management in a lightweight hybrid vehicle with fuel cells and nickel metal hydride (NiMH) batteries

Received: 21.12.2023

Accepted: 29.01.2024

Published online: 30.01.2024

Dedy Ramdhani HARAHAP [1], Wei-Chin CHANG [1*], Chun Chieh CHIU [2], Jing-Jou TANG [3]

Author's affiliations and addresses:

[1] Mechanical Eng. Dep., Southern Taiwan Univ. of Science & Technology, 1 Nantai St., Yungkang Dist. Tainan City, Taiwan 71005

[2] Metal forming technology Group, Metal Industries Research & Development Centre, 1001 Kaonan Highway, Nanzi Dist., Kaohsiung, Taiwan 81160

[3] Electronic Eng. Dep., Southern Taiwan Univ. of Science & Technology, 1 Nantai St., Yungkang Dist. Tainan City, Taiwan 71005

*** Correspondence:**

e-mail: wcchang@stust.edu.tw

tel.: *+886 6 2533131 #3560*

Abstract:

A compact electric vehicle was simulated utilizing the Advanced Vehicle Simulator (ADVISOR), a MATLAB/Simulink-based program. The primary power source for the vehicle was a 200W small Proton Exchange Membrane (PEM) fuel cell, complemented by AA-type Nickel Metal Hydride (NiMH) batteries serving as backup energy sources. Each NiMH battery had a voltage of 1.2V and a capacity of 1.9Ah. The performance of both the PEM fuel cell and the NiMH batteries was evaluated using an electronic load to meet the power requirements of the hybrid vehicle. The hybrid vehicle operated in three distinct modes: Starting Mode, Accelerating Mode, and Steady Mode, each with its specific configurations. Simulation results revealed that the batteries successfully initiated the drivetrain in the Starting Mode, while the fuel cell provided support during the Accelerating Mode. In Steady Mode, as the battery state of charge decreased, the PEM fuel cell seamlessly supported the battery and powered the load simultaneously. Various matching schemes were analyzed to meet the dynamic performance requirements of the vehicle and achieve the optimal synergy between the fuel cell and NiMH battery. The study aimed to identify the most effective configuration to ensure efficient energy management and dynamic performance in different operational modes of the hybrid vehicle.

Keywords: hybrid vehicle, PEM fuel cell, NiMH battery, energy management strategy

1. Introduction

In the realm of transportation, the escalating global demand for petroleum has driven the automotive industry to enhance power generation systems for more efficient transportation. Fuel cells have become a focal point for researchers, industries, and governments due to their capacity to generate power without emitting greenhouse gases. Widely recognized as a highly favorable and clean alternative for power generation in both mobile and stationary applications [1], fuel cells harness energy through the chemical reaction of hydrogen and oxygen from the air, tapping into an abundant resource. Among various types of fuel cells, PEM fuel cells stand out for small electronic devices, attributed to their lower operating temperatures and quicker startup times.

PEM fuel cells hold appeal for the automotive sector due to their superior energy conversion efficiencies compared to internal combustion engines (ICE), coupled with their compatibility with hydrogen. By utilizing hydrogen as fuel, fuel cells produce power and water exclusively, without emitting harmful gases into the environment. On a parallel note, batteries present an alternative energy source, offering advantages over conventional ICE vehicles, including high energy efficiency and zero pollution [2]. The optimal strategy for mitigating greenhouse gas emissions in the transportation sector involves combining fuel cells and batteries, leveraging their high energy efficiencies and minimal emissions.

Fuel cell hybridization enables the reduction of fuel cell size by incorporating a battery or an alternative power source. During periods of high-power demand, such as operating under heavy loads or during acceleration, the battery provides additional power, enhancing the overall efficiency of the fuel cell system. The utilization of the battery facilitates swift start-ups and the storage of regenerative energy. However, hybridization introduces challenges, including increased vehicle system complexity, added weight, and additional costs associated with the battery [3].

Various hybrid powertrain structures are currently available, encompassing load-following and load-leveling structures, as well as energy and power hybrid structures [4, 5]. In this study, a battery bank system was chosen to initiate energy production, followed by the utilization of hydrogen by the fuel cell to generate energy. The hybrid small vehicle under investigation incorporated a 200 W PEM fuel cell stack and a pack of 40 AA nickel-metal hydride batteries. This study involved the construction of vehicle models, fuel cells, batteries, and motors, with energy vehicle control strategies established using ADVISOR software [6]. Simulation tools prove valuable for designing and optimizing vehicle performance, aiding in the refinement of innovative models that incorporate multiple power sources and drive systems.

2. Materials and Methods

This research delves into the performance assessment of a compact electric vehicle propelled by a proton exchange membrane fuel cell (PEMFC) and nickel metal hydride (NiMH) battery, aiming to explore the practical applications of automobile technology. The work focuses on a fuel cell/battery hybrid car, specifically featuring a 200W PEM fuel cell stack and 40 AA type NiMH batteries. Each battery in the configuration possesses 1.2 volts and 1900 mAh.

The main goal of this research is to formulate an energy management strategy that optimally balances environmental impact, fuel efficiency, and dynamic vehicle performance. Leveraging ADVISOR as a fundamental tool for the initial design of fuel cell-battery hybrid vehicles, the study seeks to identify a strategy that minimizes environmental impact, lowers fuel consumption, and fulfills the dynamic performance criteria of the vehicle. The research expands upon the groundwork established in the master's study conducted by Harahap [7].

2.1. Drive train configuration

The drive train of a vehicle comprises components responsible for transmitting power to the driving wheels, excluding the engine or motor that generates this power. While the engine or motor and the drive train collectively form the powertrain, their distinct roles are noteworthy. The powertrain's

Publisher: **KOMAG Institute of Mining Technology, Poland**

primary function is to establish a connection between the power-producing motor and the driving wheels, converting generated power into mechanical force.

Given that the operating speeds of the engine and the wheels differ, maintaining optimal performance necessitates precise synchronization achieved through the application of the correct gear ratio. It is imperative to ensure that the engine operates at an approximately constant speed, irrespective of fluctuations in vehicle speed, to facilitate efficient performance. This synchronization may be achieved through automatic adjustments or manual interventions as required.

Several drivetrain configurations and energy storage technologies are employed by fuel cell vehicle developers in their cars (Fig. 1). In practice, there are four power source arrangements, each with its own set of advantages and disadvantages, depending on factors such as vehicle performance, operating conditions, control complexity, development cost, and fuel economy potential. Fig. 2 illustrates the fuel cell drivetrain arrangements and the control strategy schematically considered in this paper.

A power control strategy has been suggested to uphold overall system efficiency and monitor the state of charge (SOC) of the battery, providing insight into energy flow. The performance of the fuel cell, including power, voltage, and current over time, as well as hydrogen consumption (fuel economy), is intricately linked to the strategy employed for distributing power between the fuel cell and the battery during vehicle operation across diverse driving cycles [8].

In (a) Starting/Normal Mode, the car utilizes energy from the batteries to provide full power to the motor, as the power demand falls within the operating range, and the battery SOC remains high. In the low-speed mode (b), the fuel cell charges the battery if its SOC is below a specified threshold, simultaneously serving as the main power source for the motor. Once the power demand reaches maximum output, the battery kicks in to supply energy to the motor, supporting the fuel cell. In this mode (c), the fuel cell and the battery operate efficiently, collaborating to deliver ample power to the motor. The Steady/Charging Mode (d) involves the fuel cell exclusively charging the battery when the vehicle is stationary, requiring no power for motor generation, and when the battery SOC is low.

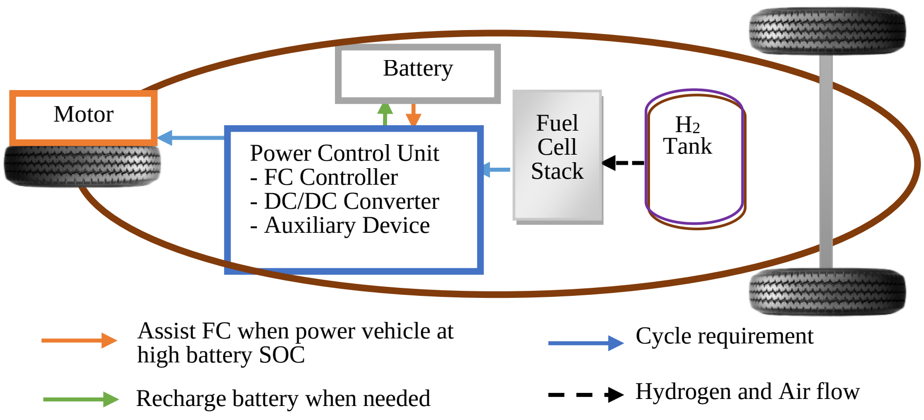

Fig. 1. Configuration of a Fuel cell hybrid vehicle

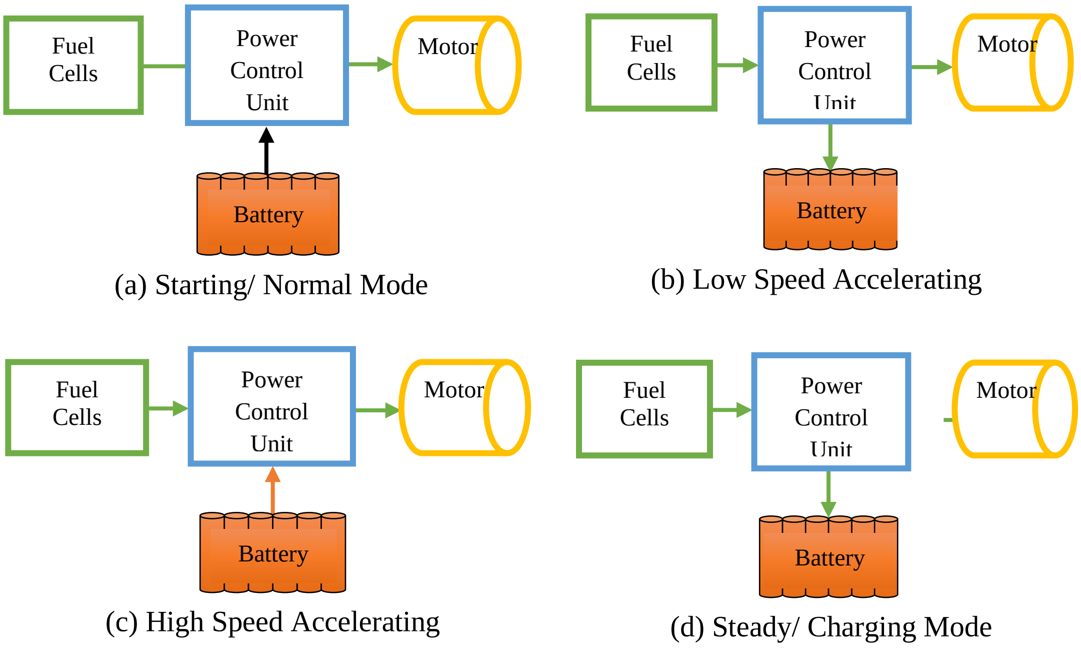

Fig. 2. FCHV drivetrain configuration control strategy

2.2. Energy Management Strategy

The control strategy, essentially an algorithm, dictates the power generation distribution between the fuel cell systems and the energy storage system during each sampling interval. Its primary goal is to maintain a power balance between the load power and the various power sources [9, 10]. Themanner in which this power split is executed can influence the minimization of hydrogen consumption. Various control techniques, addressing minimization problems, have been explored to achieve an optimal global solution.

Vehicle energy consumption occurs across three distinct modes: starting/normal mode, accelerating mode, and steady mode. The fuel cell's operating range for maximum power was constrained to 40-60%, allowing power withdrawal from the NiMH battery to maintain the fuel cell within its high-efficiency domain. Despite the low fuel efficiency, operating the fuel cell at high current density and power was necessary to propel the vehicle. Parameters such as the maximum rate of increasing fuel cell converter power (180 W/s) and the maximum rate of decreasing power (-280 W/s) were defined.

Under specific conditions, when the required vehicle power is below 20% of the fuel cell's maximum power, the battery supplies all necessary power, and the fuel cell shuts off. Conversely, if the required power exceeds the fuel cell's maximum capacity, the battery steps in to balance the power. The fuel cell activates when the battery State of Charge (SOC) reaches its low limit at 40%, and the highest desired battery SOC is set at 80%.

2.3. Determining vehicle components

The simulation employed the open-source software ADVISOR, which also supports offline usage. Widely adopted by automotive manufacturers, university researchers, and the industry, this program utilizes a MATLAB/Simulink module for modeling, simulating, and conducting dynamic system analysis. It accommodates instant, linear, non-linear systems in time domain systems, or hybrid systems through its backward and forward-facing simulation attributes [11]. The simulation process begins by configuring the vehicle model, defining driving cycle conditions, and specifying power schemes, followed by the computation of parameters within the software. Fig. 3 illustrates the ADVISOR-vehicle data settings, and additional vehicle dynamic performance parameters, including the fuel converter, energy storage, motor, transmission, wheel/axle, accessories, and powertrain, are configured on this page. These components and associated files can be saved individually, allowing for future analysis.

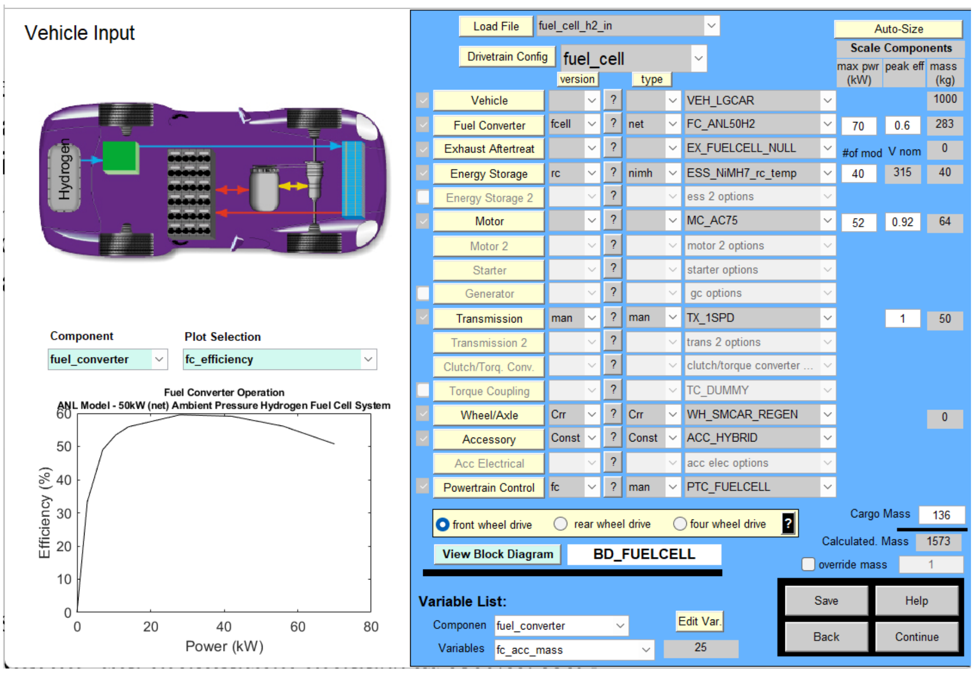

Fig. 3. ADVISOR vehicle input page

2.3.1. Fuel cells

A 200W PEM fuel cell stack was utilized to generate electricity for the motor. After testing, the stack exhibited an open-circuit voltage of 30 V, with a maximum current output of 10.49 A, resulting in a peak power of 176 W at 16.8 V (Fig. 4). The system was configured with an open-cathode design, comprising a stack of 40 cells, each featuring an active area of 19 cm^2. The pertinent parameters are detailed in Table 1 for configuration within the Advisor software.

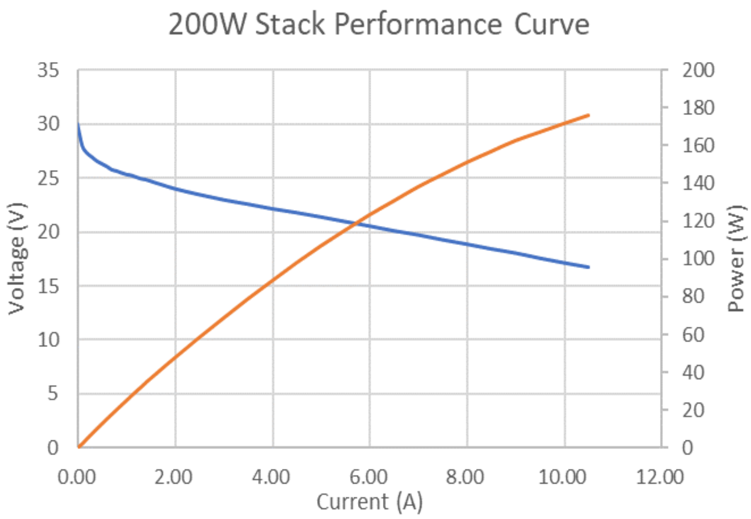

Fig. 4. Fuel cells polarization curve

Table 1. PEMFC main parameters

Parameter	Index	Unit
Number of cells	40	cell
Hydrogen pressure	0.45	bar
Flow rate at max output	2.6	L/min
Rate performance	24	V
Fuel cell power	200	Watt
Fuel cell efficiency at peak (24V)	40	%
System weight	2.63	kg

2.3.2. Energy storage systems

The energy storage system employed in this vehicle comprises a series of NiMH batteries capable of storing electrical energy generated by the fuel cell during low system load conditions and assisting the fuel cell during high system load conditions. ADVISOR provides four distinct battery models: resistive-capacity model, internal resistance model, basic lead-acid model, and neural network model [12]. The battery specifications are detailed in Table 2 and were further defined by specifying parameters like open-circuit voltage (OCV), internal resistance over temperature, and state of charge (SOC). Data for the modeling process were obtained from an analysis of an existing Panasonic Eneloop NiMH battery type AA, conducted using a Maynuo Electronic Load. Fig. 5 shows the experimental results from the electronic load use to measure the battery performances from 0.1A to 10A. From the experiment, battery performance at 5A was chosen which shows the battery voltage at 1.18V (~1.2V) with the battery capacity is 1.72 mAH and can be used for 157 s.

Table 2. Specifications of NiMH Batteries

Parameter	Index	Unit
Average voltage module	48	V
Module capacity	1900	mAh
Module mass	0.54	kg
Number of battery in series	40	pcs

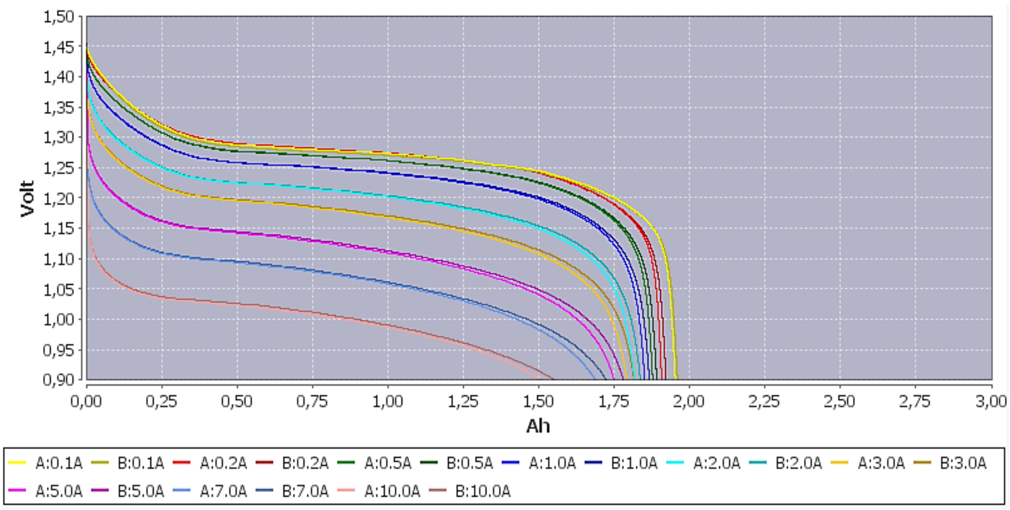

Fig. 5. Discharge curve of Eneloop BK-3MCC

Publisher: **KOMAG Institute of Mining Technology, Poland**

2.3.3. Vehicle body specification

The vehicle was conceived based on a compact fuel cell hybrid electric vehicle (FCHEV), derived from the prototype of a pure electric vehicle. The external dimensions of the prototype remain unaltered, while the powertrain undergoes a transformation, integrating a hybrid electric powertrain consisting of a fuel cell and batteries. The vehicle's configuration aligns with the ENE1-GP requirements for racing competitions in Japan [13]. This configuration ensures precise positioning of the center of mass halfway between the two axles, with traction force applied exclusively to the rear wheels. The visual representation of this vehicle is depicted in Fig. 6. Key parameters of the vehicle are succinctly summarized in Table 3.

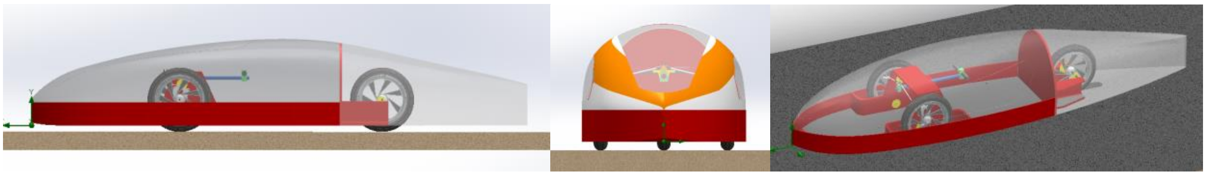

Fig. 6. Appearance of the hybrid vehicle

Table 3. The main parameters of the vehicle

Parameter	Index	Unit
Vehicle glider mass	26	kg
Vehicle full load total mass	90	kg
Cross-sectional area of the frontal vehicle	0.53	m^2
Drag Coefficient	0.19	-
Coefficient of rolling resistance	0.004	-
The tire radius	0.7	m
Maximum speed	72	km/h
Air density	1.2	kg/m^3
Drag Force	649.5	N
Drivetrain	Rear-wheel	-

2.3.4. Electric motor

The vehicle is outfitted with an in-wheel motor, specifically the Mitsuba model M0124D-V, commonly employed in lightweight electric vehicle competitions. These motors enable the direct application of torque to the wheels, precisely where it is needed, while occupying minimal space within the vehicle. The motor's performance was assessed using 48V to measure maximum torque, speed, RPM, and efficiency, with the results depicted in Fig. 7.

Table 4 shows the parameters of the motor. The motor/controller model was modified from an existing permanent magnet motor model with the average controller efficiency was set up to 90%.

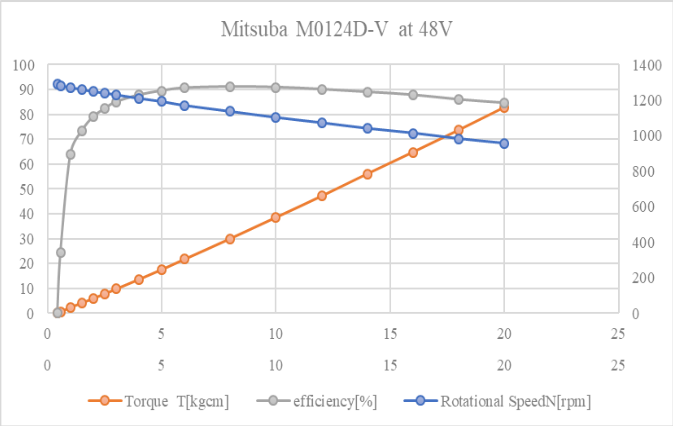

Fig. 7. Mitsuba motor performance at 48V

Table 4. Mitsuba in-wheel motor main parameters

Motor Parameter	Index	Unit
Nominal voltage	48	V
Rotational speed	1288	rpm
Nominal power	960	W
Maximum torque	8.11	Nm
Efficiency	84.5	%
Mass of motor	3.4	kg
Controller Parameter		
Nominal voltage	24	V
Voltage range	6-32	V

2.4. Model Parameters

The driving range stands out as a pivotal metric for electric cars, as a longer range enhances the car's overall utility. In this work, among the 59 driving conditions in ADVISOR, the Extra-Urban Driving Cycle (EUDC) was specifically chosen for analysis. The pertinent data regarding driving conditions is outlined in Table 5. In addition to these conditions, a customized driving profile can be incorporated, allowing for analysis of unconventional driving scenarios. The selection of the EUDC is grounded in its ability to provide a more accurate representation of real-world driving behavior, a crucial factor for competitive evaluation. The distance to be covered and the average speed serve as essential parameters to achieve optimal performance.

Fig. 8 illustrates that the test procedures necessitate a continuously variable speed. Notably, the EUDC incorporates a substantial segment characterized by extreme accelerations, reaching speeds of up to 80 km/h. It's important to note that the EUDC cycle has a maximum speed of 120 km/h, with a restriction for low-powered vehicles set at 90 km/h [14]. Information from Table 5 provides a succinct overview of driving cycle parameters, detailing test duration, distance, and target speeds. The cycle configuration was accomplished through the ADVISOR software, allowing users to either select a predefined driving cycle from the list or create a new one using MATLAB. The Simulink diagram depicted below illustrates the step-by-step process of conducting the simulation. Fig. 9 showcases the model for the fuel cell/battery hybrid vehicle within Simulink.

Publisher: **KOMAG Institute of Mining Technology, Poland**

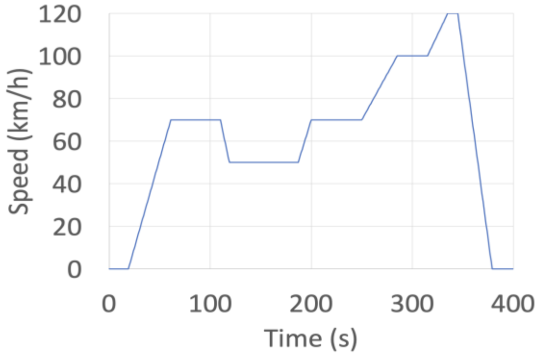

Fig. 8. EUDC cycle for light-duty vehicles

Table 5. EUDC driving condition parameters

Parameter	Index	unit
Duration	400	s
Idle time	39	s
Simulated distance	6.955	km
Maximum speed	120	km/h
Average speed	62.6	km/h
Maximum acceleration	0.83	m/s^2
Average acceleration	0.354	m/s^2

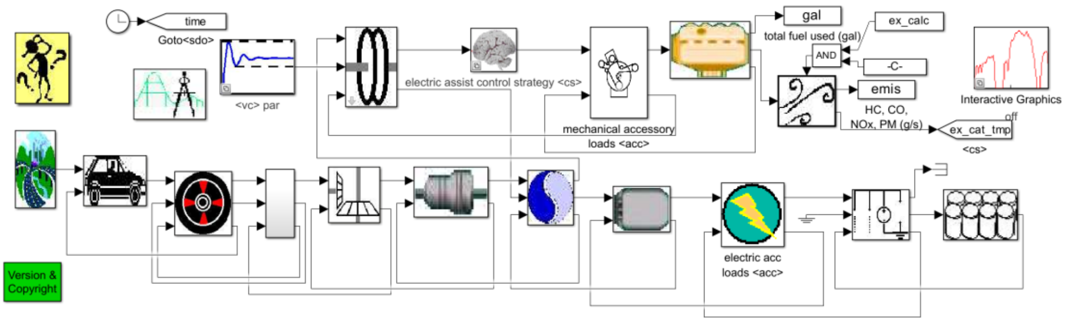

Fig. 9. The Simulink block diagram of a Fuel cell/ battery hybrid vehicle

2.5. Presenting the Analysis Findings

The ADVISOR reveals the outcomes of the analysis through graphical representations (Fig. 10), offering a comprehensive overview of vehicle performance both throughout a cycle and instantaneously at any cycle point. Summary results, including fuel economy and emissions, are presented on the right side of the window, while the left side displays detailed time-dependent results. The information displayed on the left can be dynamically adjusted to reveal various details (e.g., engine speed, engine torque, battery voltage, etc.) using pull-down menus in the upper right section of the window [15].

ADVISOR generates 150 distinct graphs post-analysis to observe the impact of the fuel cell on vehicle performance. Following the simulation, one can analyze the results as a whole or obtain subsystem-specific results separately. During the simulation, both individual data points and comprehensive data sets can be accumulated and compared. Crucial graph results from ADVISOR include fuel consumption, fuel emissions, average acceleration and speed, and maximum distance to

Publisher: **KOMAG Institute of Mining Technology, Poland**

travel. These results, aligned with dynamic vehicle performance, contribute to the fundamental design of fuel cell-battery hybrid vehicles.

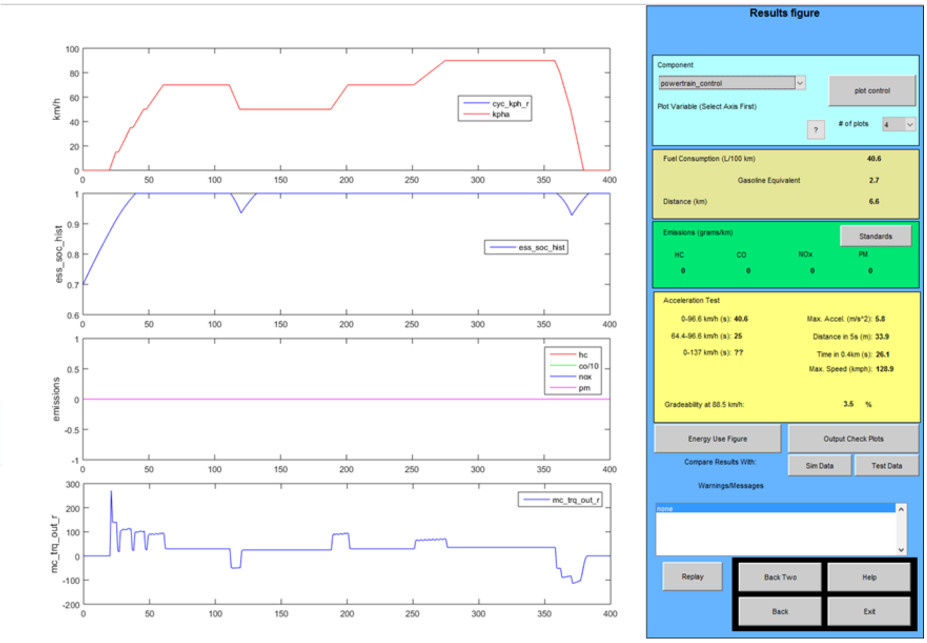

Fig. 10. Advisor results page

3. Results and Discussions

Key results were derived from ADVISOR simulations, featuring plots illustrating the velocity profile and state-of-charge (SOC) variation throughout a lap in the EUDC driving cycle. If the battery SOC falls below the desired level, the battery storage necessitates charging, and the charging power is provided by the fuel cells. Fig. 11 illustrates the SOC graph of the drive-train in this operational mode, while the vehicle's hydrogen consumption will be showcased in Fig. 12.

In Fig. 13, the average motor controller efficiency surpasses 80% during driving performance, suggesting highly favorable simulation outcomes. Beyond the ADVISOR results, the subsequent figures depict acceleration and gradeability tests aligned with EUDC driving requirements. In Fig. 14, the vehicle attains a peak acceleration of 5.8 m/s², traversing 33.9 meters in 5 seconds. Additionally, the simulation indicates that the vehicle covers a distance of 0.4 km within 26.1 seconds during the acceleration test. The vehicle's gradeability is determined to be 3.5%, affirming its ability to ascend sloping roads.

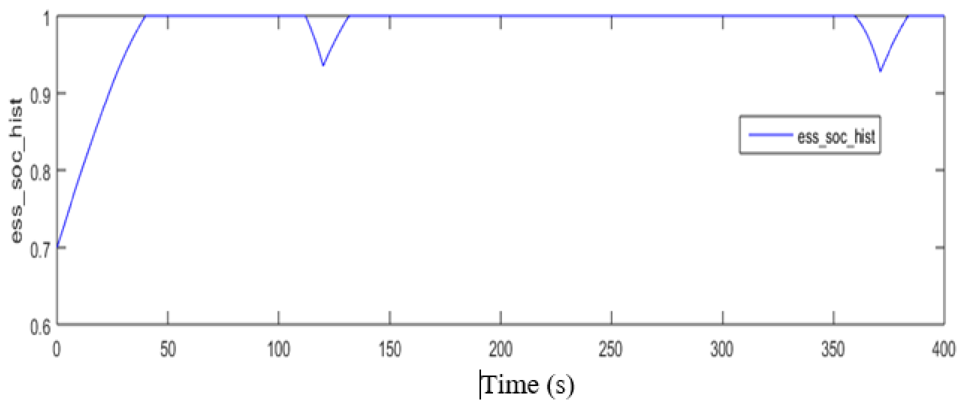

Fig. 11. Vehicle energy storage system (ESS) SOC [7]

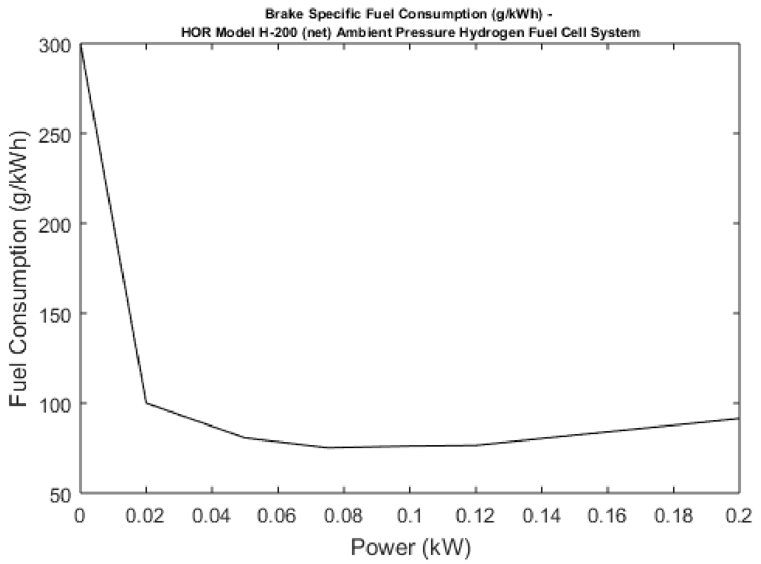

Fig. 12. Vehicle fuel consumption

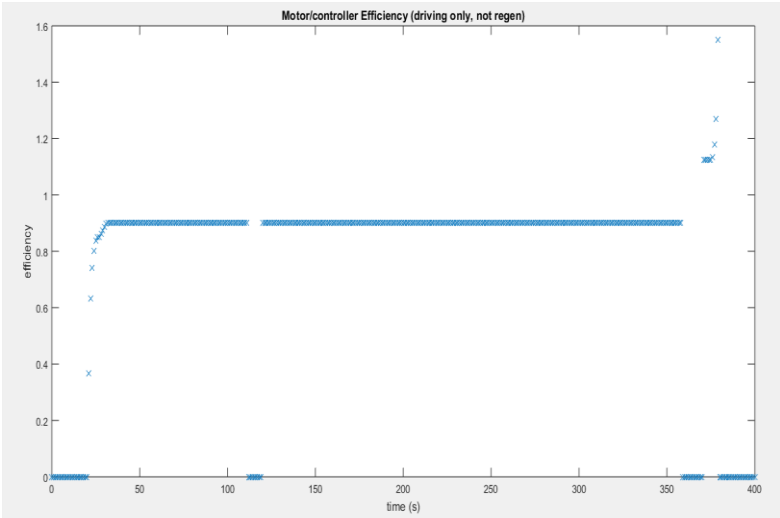

Fig. 13. Motor controller efficiency [7]

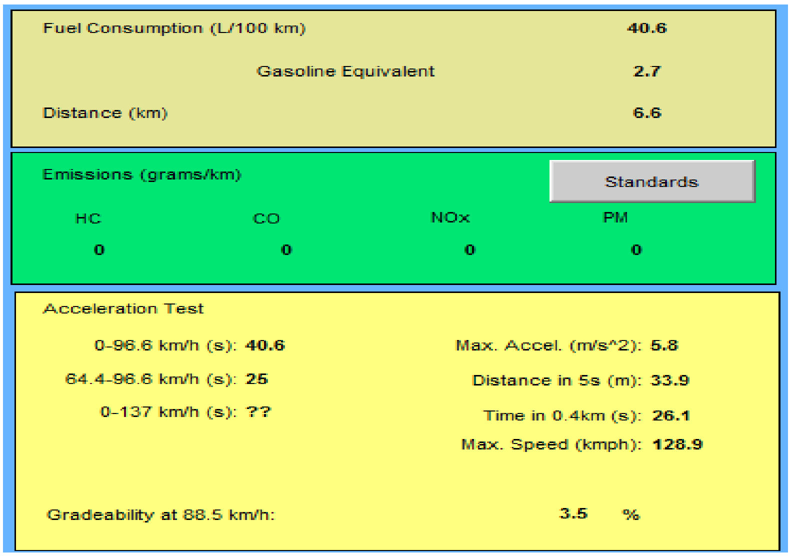

Fig. 14. Simulation results of acceleration and gradeability test

Publisher: **KOMAG Institute of Mining Technology, Poland**

4. Conclusions

In this study, an analysis of a 200W PEM fuel cell was conducted using ADVISOR. The remaining vehicle components, including the drivetrain and the Panasonic Eneloop NiMH AA-type battery selected for vehicle energy storage, were also stabilized for the analysis. The Extra-Urban Driving Cycle (EUDC) was chosen for simulation due to its suitability in replicating electric vehicle driving performance. This driving cycle closely aligns with key parameters such as distance, maximum speed, and average speed, making it comparable to other available cycles in the software.

The EUDC was utilized not only for analyzing the performance of the fuel cell hybrid car but also for internal combustion and electrically powered vehicles. The vehicle demonstrated the ability to navigate sloping roads with a 3.5% gradeability, achieving a fuel consumption of approximately 40.6 L/100 km over a distance of 100 km. Accelerating to 33.9 m took 5 seconds, while covering 0.4 km required 26.1 seconds. The simulation effectively illustrates the dynamic system and control strategy embedded in the software, providing a comprehensive evaluation of the power and fuel economy performance of the fuel cell-battery electric hybrid vehicle. The results from the vehicle prototype simulation further confirm its adherence to design requirements.

Acknowledgements

The corresponding author would like to thank the Metal Industries Research & Development Centre (MIRDC), Taiwan for their financial support on this work.

References

[1] Tie, S.F., Tan, C.W.: A review of energy sources and energy management system in electric vehicles. Renewable and Sustainable Energy Reviews, 2013. 20: 82-102. DOI: https://doi.org/10.1016/j.rser.2012.11.077

[2] Wang, Y., et al.: Power management system for a fuel cell/battery hybrid vehicle incorporating fuel cell and battery degradation. Int J Hydrogen Energy, 2019. 44: 8479-8492. DOI: 10.1016/j.ijhydene.2019.02.003

[3] Dong, Q., et al.: Cost, energy, and carbon footprint benefits of second-life electric vehicle battery use. iScience, 2023. 26(7): 107195. DOI: https://doi.org/10.1016/j.egypro.2016.12.065

[4] Wu, J., et al.: Comparative Analysis on the Rule-based Control Strategy of Two Typical Hybrid Electric Vehicle Powertrain. Energy Procedia, 2016. 104: 384-389. DOI: https://doi.org/10.1016/j.egypro.2016.12.065

[5] Das H.S., Tan C.W., Yatim A.H.M.: Fuel cell hybrid electric vehicles: A review on power conditioning units and topologies. Renewable and Sustainable Energy Reviews, 2017. 76: 268-291. DOI: https://doi.org/10.1016/j.rser.2017.03.056

[6] https://sourceforge.net/projects/adv-vehicle-sim/ [accessed: 12.15.2023]

[7] Harahap D.R.: Research on Energy Management Strategy for PEMFC/ Nickel Metal Hydride (NiMH) Battery Hybrid Vehicle. Master thesis of Southern Taiwan University of Science & Technology, Taiwan. 06.2017.

[8] Zhao, H., et al.: Comparison of Hybrid Fuel Cell Vehicle Technology and Fuel Efficiency. Research report UCD-ITS-RR-11-10, University of California, Davis, 2011.

[9] Rosario L.C.: Power and Energy Management of Multiple Energy Storage Systems in Electric Vehicles. PhD. Dissertation of Cranfield University, UK. 06.2007.

[10] Zhao, X., et al.: Energy management strategies for fuel cell hybrid electric vehicles: Classification, comparison, and outlook. Energy Conversion and Management, 2022. 270: 116179. DOI: https://doi.org/10.1016/j.enconman.2022.116179

[11] Kunt M.A.: Advisor-Based Modelling of a Passenger-Type Fuel Cell Vehicle and the Effect of Movement Resistances on Battery Performance", ECJSE, 2022, 9 (1): 189-202. DOI: 10.31202/ecjse.956474.

[12] Williamson S. S.: Energy Management Strategies for Electric and Plug-in Hybrid Electric Vehicles, Springer 2013. ISBN 9781461477105.

Publisher: **KOMAG Institute of Mining Technology, Poland**

[13] https://www.suzukacircuit.jp/ene1-challenge/ [accessed: 12.15.2023]

[14] New European Driving Cycle - Wikipedia, https://en.wikipedia.org/wiki/New_European_Driving_Cycle [accessed 12.17.2023]

[15] Markel T., et al.: ADVISOR: a systems analysis tool for advanced vehicle modeling," Journal of Power Source, 2002, 110: 255-266. DOI: https://doi.org/10.1016/S0378-7753(02)00189-1

Publisher: **KOMAG Institute of Mining Technology, Poland**

https://doi.org/10.32056/KOMAG2023.4.6

System of current collectors inertization for safety use in explosive atmosphere-testing and results

Received: 05.01.2023

Accepted: 29.01.2024

Published online: 30.01.2024

Author's affiliations and addresses:

[1] KOMAG Institute of Mining Technology, Pszczyńska 37, 44-101 Gliwice, Poland

[2] RWTH Aachen University, Templergraben 55, 52062 Aachen, Germany

*** Correspondence:**

e-mail: adrwiega@komag.eu

Andrzej DRWIĘGA [1*], Krzysztof LESIAK [1], Elisabeth CLAUSEN [2], Maximilian GETZ [2]

Abstract:

R&D work regarding the innovative mine transportation system, planned to be powered by the three-phase busbar, developed within the RFCS project "Increase of mines efficiency and health protection through the innovative transport system based on BUSDUCT" is discussed. Assumptions regarding the construction of the locomotive and the production of nitrogen from the air for inerting purposes are discussed in the first part, whereas in the second part adapting the current collector's brushes to nitrogen injection, the relevant CFD calculations, the stand for testing the inertization, are presented. Many interesting experiments on the effectiveness of inertization using explosive mixtures of hydrogen and air are illustrated, described and discussed.

Keywords: monorail locomotive, suspended busbar, current collectors, methane atmosphere, brush inertization

Publisher: **KOMAG Institute of Mining Technology, Poland**

1. Introduction

R&D work based on the "Mid-Term Report" of the project "Increase of mines efficiency and health protection through the innovative transport system based on BUSDUCT" [1] is discussed. The project, led by ITG KOMAG in 2019-2021, was carried out in a consortium of 5 partners, whereas three of them from Poland i.e. KOMAG, BECKER-Warkop and PGG, one from Germany i.e. RWTH Institute and BARTEC company from Slovenia. Completion was expected in 2022, but the project was terminated, as a result of doubts related to market demands for the proposed solution in the context of mine closures. Additionally the experts supervising the project also had doubts about the safe use of the proposed solution in the conditions of methane mines.

The idea of the BUSDUCT project resulted mainly from the situation of the mining industry in Poland, where the transport routes are becoming longer in a result to reach the next coal seams, which are more and more distant from the shaft, whereas building new shafts in terms of the policy of reducing the importance of coal as an energy source is unjustified. An efficient mine transportation system was perceived as very important for the effective functioning of currently operating mines. The commonly used, diesel powered locomotives are onerous due to exhaust gases and heat emission in confined space. Limited speed extends the exposure time of miners to exhaust gases and results in a significant shortening of their effective worktime. The development of the innovative mine transportation system based on a three-phase busbar, for powering the suspended locomotives, complies with the EU Directive [2] ATEX 2014/34/EU [3], standards [4-6] was a project purpose.

According to the Polish legislation, mine workings are divided into three categories: "a", "b" and "c". In mine workings "c", despite active ventilation, the methane concentration may exceed 1%. The main goal of the proposed innovation was the possibility of using such a system in all mine workings even those with the highest risk of methane explosion. The planned transport system offers the following advantages:

- Health protection of miners by elimination of diesel exhaust gases from the underground atmosphere, improvement of work comfort due to limitation of temperature increase in mine workings.
- Higher mine profitability due to increased disposable work time of miners, constant availability of the electrically powered suspended locomotives, with no refueling breaks.
- Up to 65% energy savings and energy recuperation during downhill transportation.
- Possibility of parallel operation in the same time of several locomotives with no danger of exceeding CO concentration in mine workings.

The above advantages could be achieved when the prototype, ready-to-be-produced for the transport system is launched, what was expected as the result of the project, however as mentioned, the project was earlier terminated. Nevertheless, the prototype of the nitrogen generator and the developed dedicated current collector is innovative and technically interesting that the authors decided that it is worth presenting it in the article to share the acquired knowledge in the field of nitrogen separation from air and the method of current collector's brushes inertization.

2. Planned transportation system and its safety case assumptions

Two current collectors (CC) were decided to use for the planned suspended machine. Each current collector has four brushes, working by contacts with the 3-phase busbar at the speed of up to 4 m/s, which results from the assumed maximum speed of the suspended machine. The unavoidable sparking of the brushes creates a huge risk of initiating an explosion. To ensure the safe operation of the current collectors of the planned suspended monorail machine an inertization of brushes contact area was planned. It was also necessary to take into account the maximum speed of air of 8 m/s in the workings.

At the beginning the consortium chose the type of busbar, taking into account the practical aspects, mainly economic, so that for long routes the cost is acceptable to future users. The selected busbar offered by the Conductix company [7] is shown in Fig. 1.

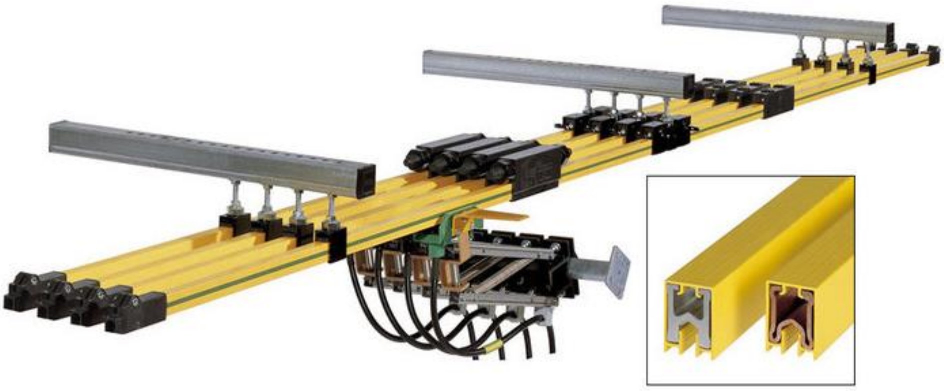

Fig. 1. View of the selected type of busbar [7]

The standard for the explosion protection method “pressurized enclosure” EN-IEC 60079-2 [5] is used as a technical rule, however the standard cannot be applied directly to the mobile devices. Due to possible sparking, the contact zone of the brushes and the busbar lines has to be isolated from the mine atmosphere, which can contain explosive concentration of methane. For that purpose inertization of the current collector working zone, by injecting nitrogen, resulting the overpressure inside the brush collector, separated from the atmosphere by a special aggregate subassembly, were developed. Furthermore, to ensure a safe operation, nitrogen injection to the current collectors should be controlled by a series of sensors. The scheme of the concept of the inertization system is illustrated in Fig. 2.

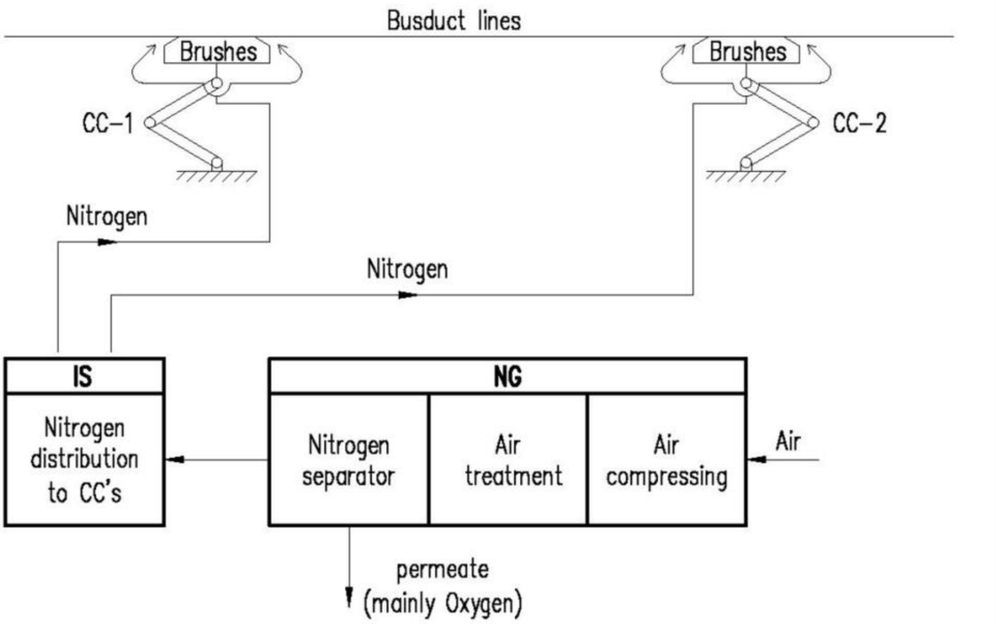

Fig. 2. Block diagram of the brushes inertization [1]

The following sensors were used to control the inertization system:

– Pressure measurement devices to control the minimum overpressure inside the single brush collector,
– Volumetric flowmeters to monitor the nitrogen supply to each brush collectors.

ATEX certification of the type: I M1 Ex ia I Ma is a main requirement for all sensors to be installed in the prototype.

The scheme in Fig. 2 presents an overview of the blocks of the NG nitrogen generator and the IS inerting system. The NG uses a membrane technology, which was chosen as the most advantageous due to necessity of meeting the requirements of the ATEX directive and the requirement of mobility. As the separation of gases to produce nitrogen takes place at the molecular level [8, 9], the air supplied to the separator must be specially treated. The requirements are related to the content of moisture, solid particles and oil aerosols, that got into the air during its compression. The residual oil content must be below 0.01 mg/m^3. The ambient (atmospheric) air is compressed, carefully filtered, and then passed through a series of separation modules consisting of thousands of membrane fibres. The fibres separate nitrogen from air. The separation follows the principle of selective gas permeability through the membrane walls. Smaller gas molecules (water, carbon dioxide, oxygen and argon), which have high permeability, pass faster through the membrane fibres than the larger, less permeable molecules of gases such as nitrogen and methane. The purity of the nitrogen obtained by this method ranges from 95 to 99.5% but a higher purity results in a lower nitrogen output. According to preliminary calculations, it was possible to design a generator with a separated nitrogen efficiency of approximately 3 l/s in a given size. Since 8 brushes were assumed to be inerted, this efficiency for one brush guaranteed 0.375 l/s of nitrogen.

The nitrogen generator pumps nitrogen to the pressure tank in the inertization system IS consisting of two units, composed of several parts, including pressure reducing valve and pressure sensors. The unit shown in Fig. 3 distributes nitrogen to the four brushes of the one current collector (CC-1) and the same second unit distributes nitrogen to the second current collector (CC-2). Each current collector has 4 brushes. First, nitrogen is directed to the reducing valve, where the pressure is reduced to a constant level (set at the start-up). Nitrogen of the reduced pressure is directed through the flowmeter to the distributor, where it is distributed to each brush of the current collector.

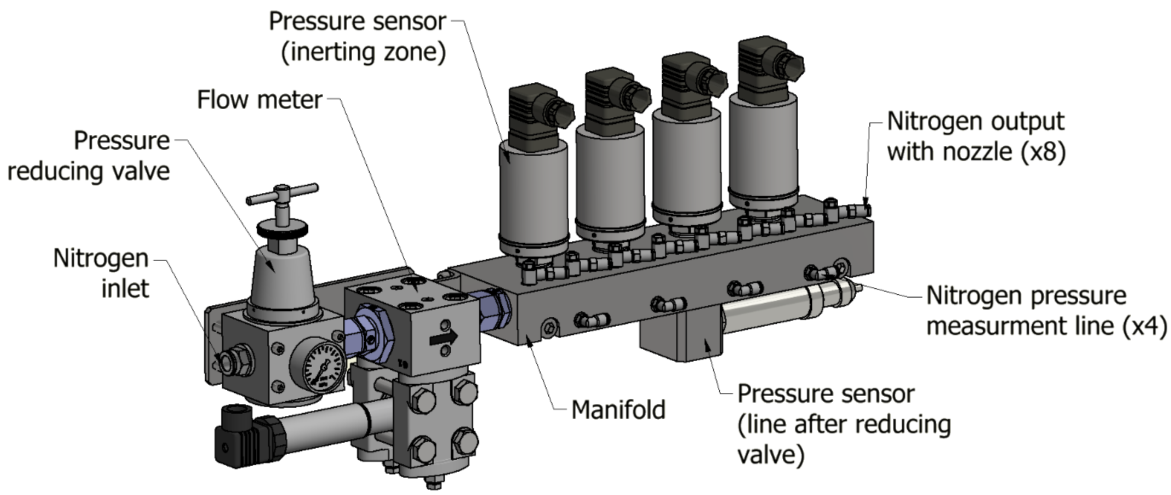

Fig. 3. Nitrogen inertization system unit [1]

3. Testing and results

The initial solution of the inerted brush, is shown in Fig. 4. The main idea was to use sliding scrapers (2) on both sides of the brush (1) due to the bidirectional sliding of the brush on the busbar line (7). The sliding scraper's task was to initially isolate the brush from the atmosphere. The scrapers (2) have channels with nozzles (4) at the end, that supply nitrogen to the brush working zone, delivered from the nitrogen inertization system unit (Fig. 3) through the thin tubes (5). In addition the longitudinal side covers (3) and typical brush cover (6) were taken into consideration.

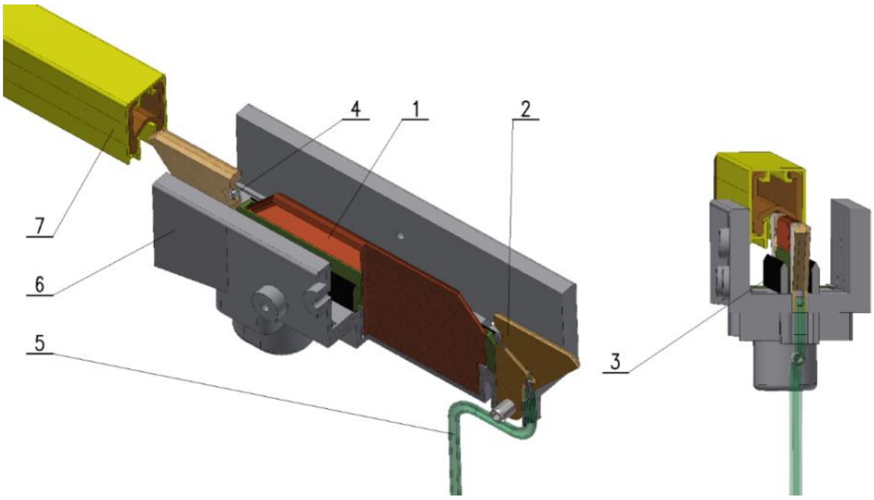

Fig. 4. Model of the solution of inerted brush [1]

Further, a CFD calculation model was developed to determine the assumptions of the nitrogen feed rate regarding the assumed maximum nitrogen efficiency 3l/s i.e. 0,375 l/s per one brush. The simulations, an example of which is illustrated in Fig. 5 show, that building up an overpressure inside the each brush collector is possible with the given seals. However, they also show that it is not yet possible to reach the minimum overpressure at every location inside each brush collector of the present design of the brush collector. That is why the additional sealing was needed.

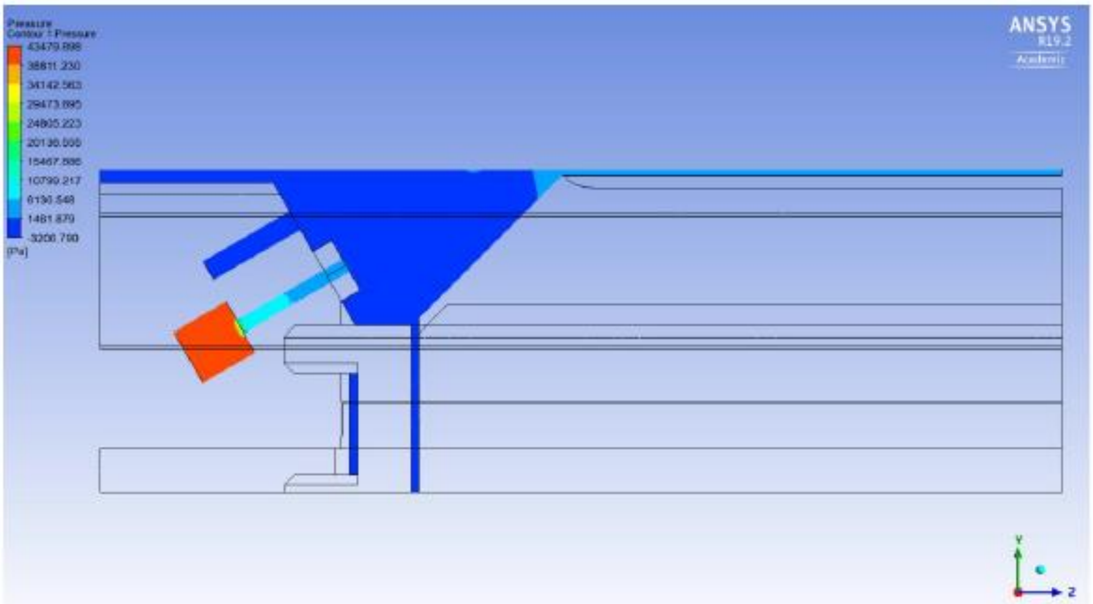

Fig. 5. 2-dimensional overpressure contour result of the CFD simulation on the single brush with using a nitrogen nozzle diameter of 1.0 mm and a 0.15 l/s inlet of nitrogen [1]

The additional wheels with rubber tire, before the scrapers on both sides of the brush, was proposed. The advantage of using the rotating rubber tire is that it better adapts to the shape of the electric track and therefore provides better sealing. As it can be seen in Fig. 6, CFD calculations with such additional rubber tyres give the positive impact. The tire reduces ingress of external atmosphere to the brush to dozen or so percent. The effect of double protection was achieved, which can be compared to the double door windbreak system. As a result the final solution of inerted brush, shown in Fig. 7 has been accepted by the consortium.

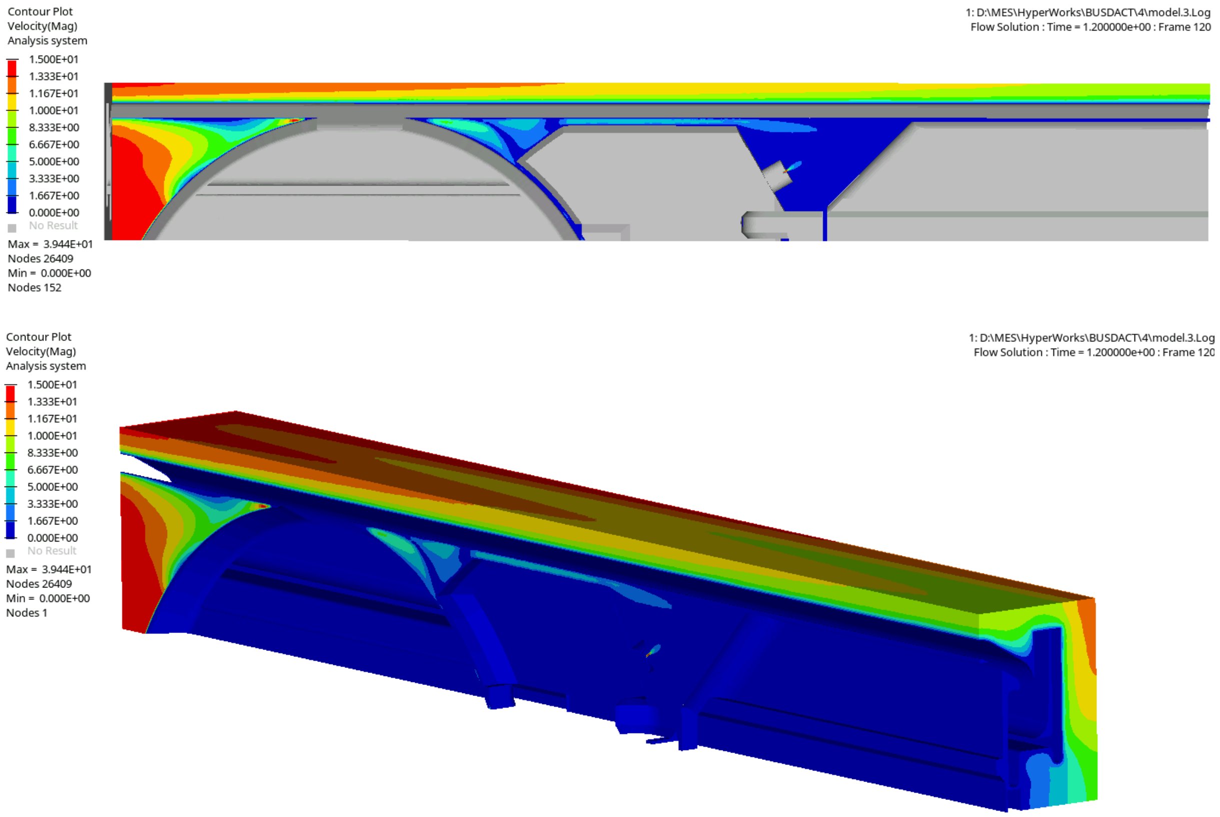

Fig. 6. Illustration of CFD modelling of inertization results- air speed map [1]

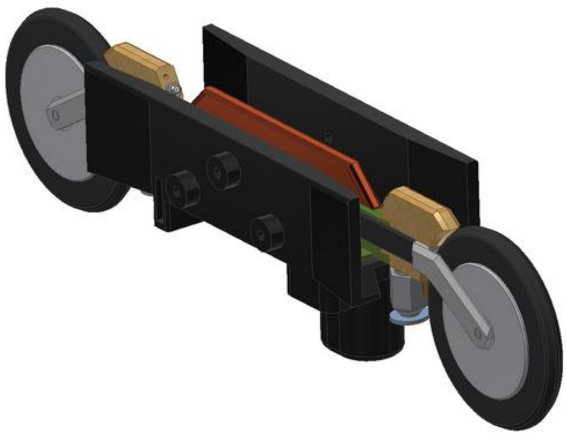

Fig. 7. Model of the final solution of inerted brush retrofitted with additional wheels with rubber tyres on both sides [1]

The next R&D proceeding was to check inertization of the brush efficiency in practice. It was decided to test the brushes during their inertization in the explosive atmosphere. For this purpose it was decided to use a hydrogen mixture, which is reliably explosive at various concentrations, unlike methane mixtures, therefore, the certainty of the experiment was essentially 100%. The special, transparent, two-compartment hydrogen mixture container (HMC) was designed. The hydrogen mixture could move in this container in a closed circuit in the upper and lower compartment thanks to three small fans with adjustable rotational speed up to 20,000 rpm illustrated in Fig. 8 installed inside the upper compartment of the container. The speed of the mixture up to 8m/s was used to reflect the maximum air speed in the mine workings [10].

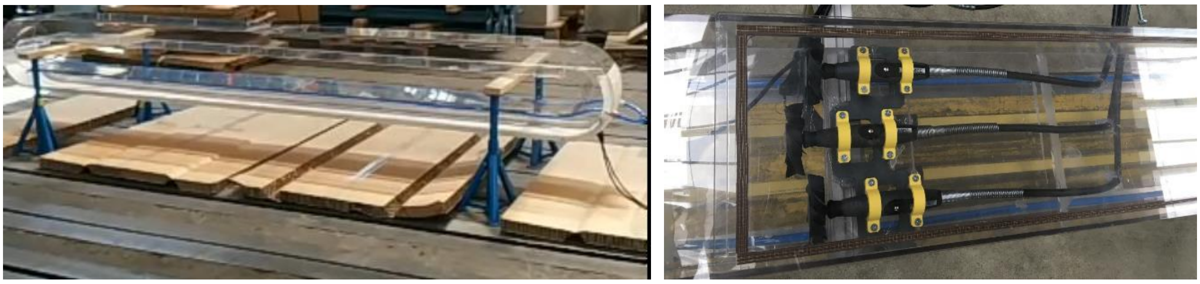

Fig. 8. The transparent two compartment container HMC (on the left), three fans with adjustable speed up to 20,000 rpm installed inside the upper HMC compartment [1]

The trolley equipped with brushes moved along a C-section route placed on the floor. In Fig. 9 it can be seen the route, the trolley equipped with two brushes installation and two busbar lines over the trolley. A speed of the trolley ranging from 0.78 m/s to 4 m/s was used during the tests to reflect the possible speed of the suspended locomotive.

Fig. 9. The trolley with two brushes installation on C-section route on the floor (left), the brushes applied to the busbar lines during nitrogen pressure testing (on the right) [1]

Two busbar lines have been passed through the lower compartment (Fig. 10) Each trolley pass experiment required sealing the lower compartment of the HMC using stretch foil to keep the hydrogen mixture inside before the trolley's pass.

Fig. 10. View of the transparent container, two busbar lines running across, the trolley on the C-section route below [1]

In Fig. 11 the scheme of the test stand is presented. The brushes on the trolley were electrically connected, so the circuit of the 55 kW dyno-motor was closed through the two lines of busbar and brushes on the trolley. Thus assured that the electric current in the busbar and brushes was adequate to the current in the planned system.

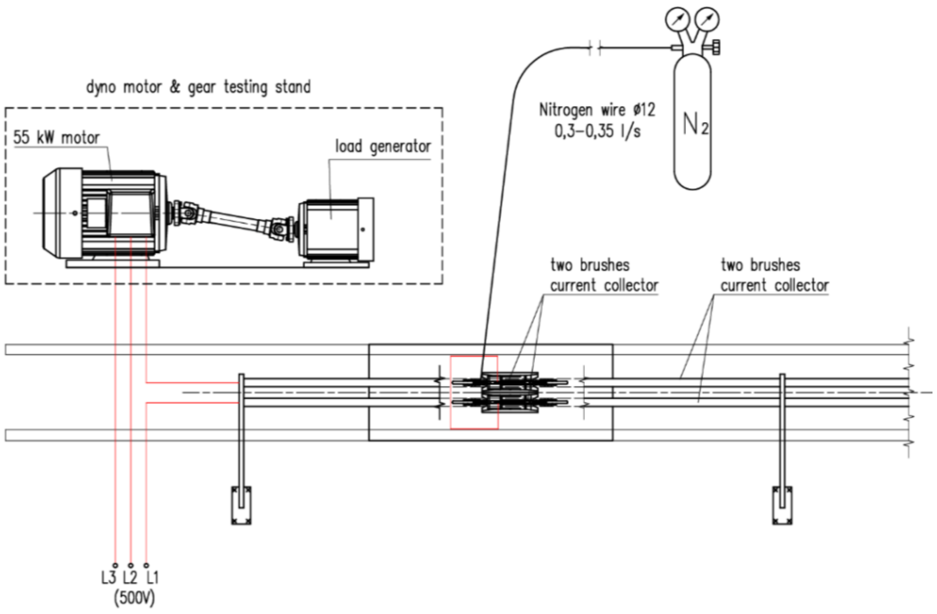

Fig. 11. Scheme of the test stand for inertization efficiency testing [1]

With the help of a high pressure nitrogen cylinder, this gas was fed to the brushes via a 20 m hose. A valve reducer was used to control the nitrogen supply. The first part of the test process dealt with the determination of suitable hydrogen concentrations to enable controlled explosions inside the hydrogen mixture container (HMC). An iterative approach was chosen for determining this concentration. In the experiments, hydrogen-air mixtures with a variable hydrogen content were ignited. Experiments with hydrogen-air mixtures containing 40-50 vol.% of hydrogen lead to explosions that exerted too much mechanical strain on the container, however its loose covers well contributed to dissipation of the explosion energy. The impact of the explosion is given in Fig. 12. The top covers of the HMC were thrown to height of several centimeters.

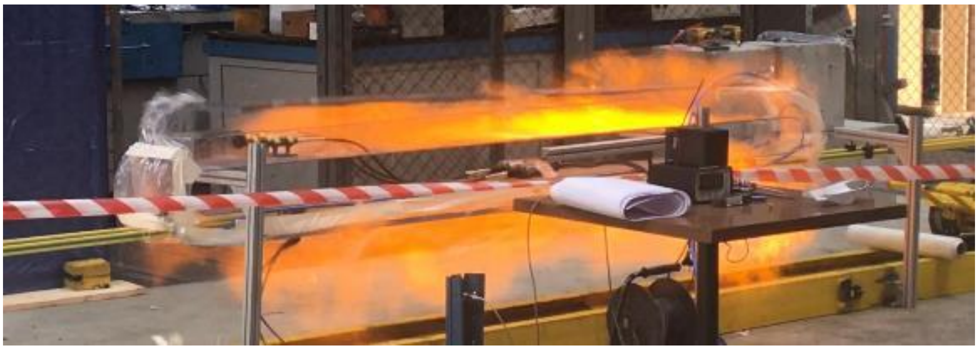

Fig. 12. View of the effect of the explossion, when nitrogen was not used for the brush inertization and the hydrogen concentration was around 30% [1]

Literature analysis [11] and testing the hydrogen mixture concentrations gave the following cognizance. Hydrogen concentration of 20 vol.% proved to be too low as an ignition of the mixture did not reliably occur. A hydrogen-air mixture with 30 vol.% of hydrogen proved to be suitable. No visible damage on the container could have been observed and explosions occurred reliably. The top loose covers of the HMC container were thrown upwards typically by approximately 15 cm, however it happened even by several dozen centimeters, during the explosion.

In the next step, it was decided to test the pressure in the area of the inertized brush in a dynamic way, while the trolley is moving on the test stand. A pressure sensor [8] was installed to one of

Publisher: **KOMAG Institute of Mining Technology, Poland**

the brushes through a vertical hole drilled in the middle of the brush. The sensor used to measure overpressure gives a feedback voltage which is proportional to the measured pressure. To determine the amount of nitrogen flowing to one inertizated brush, reference was made to the planned capacity of the nitrogen generator i.e. 3 l/s. This amount of nitrogen is designed for two CCs, i.e. 8 brushes, thereby the amount of nitrogen per one brush is 3: 8 = 0.375 l/s, which makes 22.5 l/min. It was also assumed that the actual amount of nitrogen supplied to a single brush may be slightly lower than the nominal one, therefore the inertization efficiency tests were carried out for the flow of 20 l/min and 15 l/min. Two graphs for both amounts of supplied nitrogen are shown below. Graphs of relatively low driving speeds were selected due to the most visible characteristic points of the route. The graphs are shown in the Fig. 13 and Fig. 14.

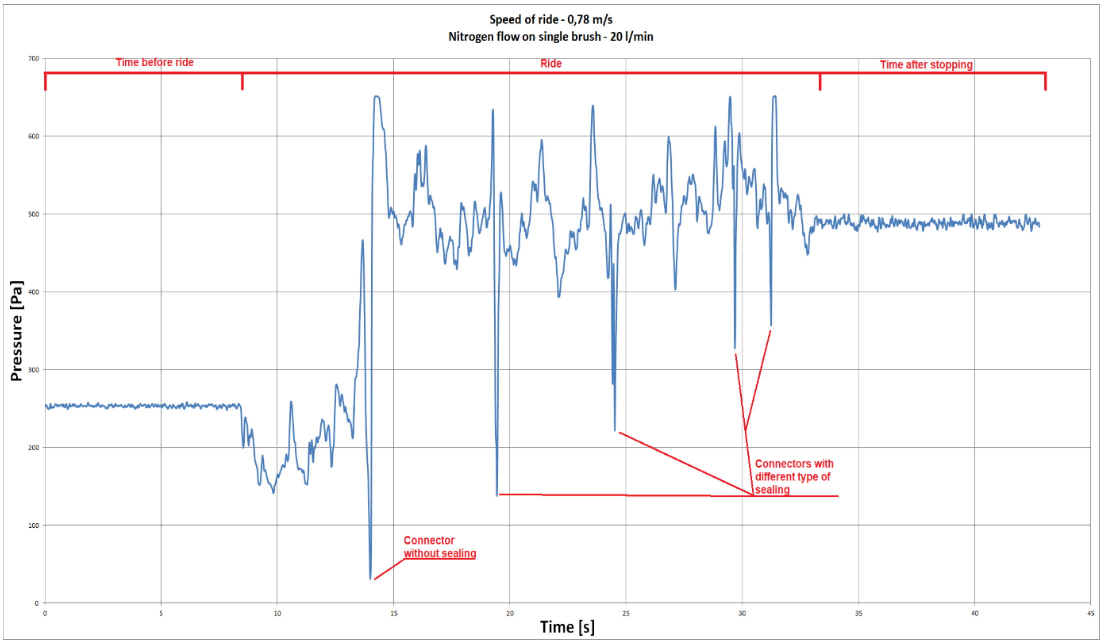

Fig. 13. Graph of pressure of inerting zone – 0,78 m/s & 20 l/min [1]

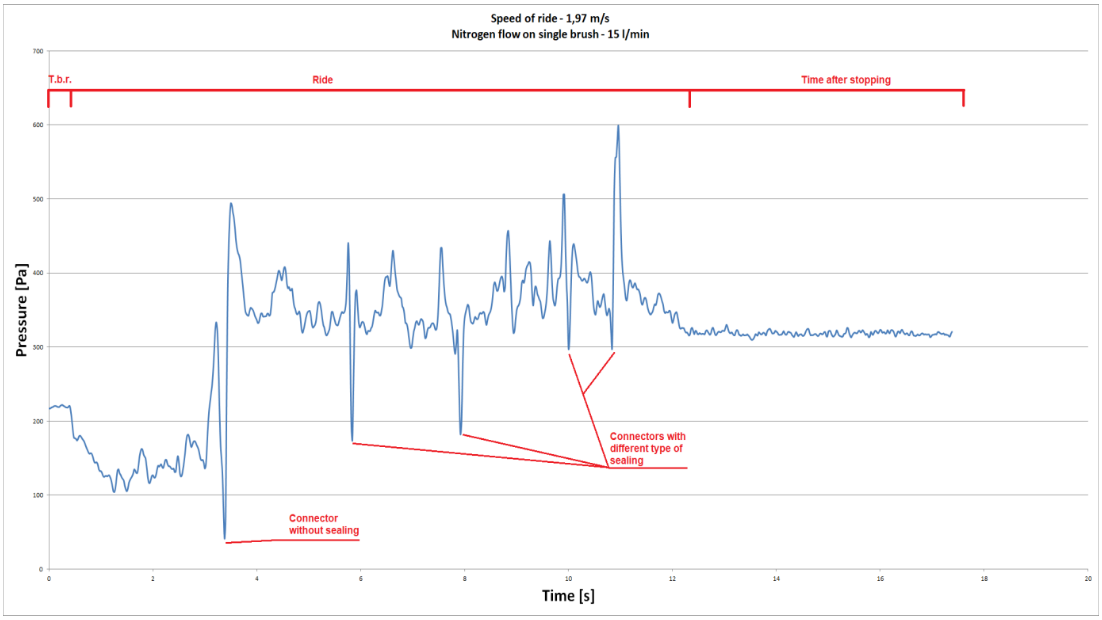

Fig. 14. Graph of pressure of inerting zone – 1,97 m/s & 15 l/min [1]

The graphs show the difference between the pressure at the start and end points of the driving cycle. This is visible in all tests for various speeds. This may be the result of shifts between the busduct lines components. During the driving cycle, the inertization pressure is kept in a relatively stable range. The pressure drops on the busduct connectors are clearly visible. The first - the largest drop is shown by the connector without the use of seals. The next ones present various types of seals, ranging from plastic inserts, through self-adhesive EPDM sponge, ending with the combination of EPDM with polyurethane foam. The tests show that with the use of seals on rail connectors, the inertization pressure remains within satisfactory limits.

Subsequent tests determined the necessity of spark excitation inside the cover for triggering an explosion. The container was filled with a hydrogen-air mixture containing the previously determined 30 vol. % of hydrogen. During the tests, even without inertization, no explosions occurred. This indicated that spark excitation between brushes and busbar lines was necessary. The spark excitation was realised by applying 8 cm long insulating strips to the single busbar lines. The strips cause a temporary loss of electrical contact. When the electrical contact is restored sparks occur as planned.

After preparing the test stand with the mentioned insulating strips, three experiments were conducted without inertization. Every one of the three tests led to an explosion. Another preparatory test was to check if the explosive mixture inside the container stays explosive for the preparation time of the test bench. The preparation time for one test is 30 s. This is the time the testing team needs to be ready for conducting a test.

To check if the explosibility can be ensured after 30 s, 3 tests were conducted with a spark generator. 30 s after the container is filled with the flammable hydrogen-air mixture sparks are generated inside it to trigger an explosion.

During testing the crew of six persons was involved with the following tasks:

1. Operating the dyno test stand to supply 500V voltage and loading to the phase connected to the single bus duct lines,
2. Operating the rope pull device to drive the trolley,
3. Operating the nitrogen supply system,
4. Operating the hydrogen supply,
5. Operating the rotational speed of fans inside the container,
6. Supervising the activities.

Due to the risk of electric shocks and the explosion of the hydrogen mixture, the testing stand was under special supervision. Persons not involved in the tests had no access to the area of the test stand. Every time after passing through the HMC and braking the trolley was retracted manually. During this operation, the power supply of the busbar lines was turned off. The tests were realized for the speed of the CC of 1 m/s, 2 m/s and 4 m/s and for the mixture flow speed of 4 and 8m/s, what makes 3 x 3 = 9 speed variants. The basic assumptions to confirm the efficiency of inertization for each speed variant were as follows:

1. explosion was result in each test when nitrogen for inertization was not used
2. there was not explosion in each test result when nitrogen for inertization was used.

If a positive evaluation for the above is achieved, the inertization system is considered efficient.

The tests were realized with the developed sealing set of the brushes manufactured by KOMAG by using 3D printers of FDM technology. ABS and PLA filaments were used in the manufacturing process. The tests were realized for two variants of CC speed: 1 m/s and 4 m/s. The mixture speed inside the cover was 8 m/s for all experiments. All completed tests confirmed good efficiency of the proposed inertization system as all experiments with inertization resulted in lack of explosion while all experiments without inertization resulted in an explosion.

Publisher: **KOMAG Institute of Mining Technology, Poland**

4. Conclusions

The tests on the inertization efficiency of the current collector brushes at the KOMAG test stand confirmed the reliability of the inertization system in combination with the brush seals. This means that all tests with use of inertization did not cause an explosion when nitrogen was supplied and all attempts resulted in an explosion when no nitrogen was supplied. This testing procedure gives confidence that the inertization is effective. It should be emphasized here that the explosive mixture was prepared not using the methane but using hydrogen, which strengthens the credibility of the test results and provide the basis for the planned transportation system.

Although the system has not been fully implemented due to the earlier termination of the BUSDUCT project, the use of the inertization system in other solutions for devices operating in potentially explosive atmospheres cannot be ruled out. A nitrogen generator, which is not the subject of this article, with an output of 3 l/s, has also been successfully implemented and can be used in other R&D work.

References

[1] Mid-Term Report "Increase of mines efficiency and health protection through the innovative transport system based on BUSDUCT" Reporting period: 1st June, 2019 – 30th November, 2021 (unpublished)

[2] DIRECTIVE 2014/34/EU of the European Parliament and of the Council of 26 February 2014 on the harmonisation of the laws of the Member States relating to equipment and protective systems intended for use in potentially explosive atmospheres (recast) (Text with EEA relevance). (Official Journal of the European Union L 96, 29.3.2014, p. 309–356)

[3] Guidelines to Directive 2014/34 EU - ATEX 'Product' Directive. Fourth edition of the guide to the application of directive 2014/34 EU on the harmonisation of the law of the Member States relating to equipment and protective systems intended for use in potentially explosive atmospheres, published in November 2022

[4] Standard EN IEC 60079-0:2018 Explosive atmospheres – Part 0: Equipment – General requirements

[5] Standard EN 60079-2:2014 Explosive atmospheres – Part 2: Equipment protection by pressurized enclosure "p"

[6] Polish Standard PN-G-50090:1997 Work protection in mining industry - Electric network of wire traction - Requirements

[7] Szynoprzewody (Busbars), https://www.conductix.pl/pl/produkty/szynoprzewody/szynoprzewody-pojedynczo-izolowane?parent_id=11404 [accessed: 18/12/23]

[8] Hu T., Zhou H., Peng H., Jiang H.: Nitrogen production by efficiently removing oxygen from air using a perovskite hollow-fiber membrane with porous catalytic layer., Front. Chem., 2018, Sec. Chemical and Process Engineering, Volume 6, 329 https://doi.org/10.3389/fchem.2018.00329 [accessed: 19/12/23]

[9] Baker R. W., Low B. T.: Gas separation membrane materials: a perspective. Macromolecules, 2014, 47, 6999–7013. https://doi.org/10.1021/ma501488s

[10] Przewietrzanie kopalń - Materiały dydaktyczne do użytku wewnętrznego) *(Mine ventilation - Teaching materials for internal use)* https://czek.eu/strona%20eksploatacji%201/rozdzialy/17%20przewietrzanie.htm#_Toc535520404 [accessed: 19/12/23]

[11] Schröder V., Holtappels K.: Explosion characteristics of hydrogen-air and hydrogen-oxygen mixtures at elevated pressure. 2005. http://conference.ing.unipi.it/ichs2005/Papers/120001.pdf [accessed: 19/12/23]

Publisher: **KOMAG Institute of Mining Technology, Poland**